Research Paper

GEOSPHERE

GEOSPHERE, v. 15, no. 3

https://doi.org/10.1130/GES02027.1

22 figures

CORRESPONDENCE: steffen.bergh@uit.no

CITATION: Bergh, S.G., Sylvester, A.G., Damte, A., and Indrevær, K., 2019, Polyphase kinematic history of transpression along the Mecca Hills segment of the San Andreas fault, southern California: Geosphere, v. 15, no. 3, p. 901–934, https://doi.org/10.1130/GES02027.1.

Science Editor: Shanaka de Silva
Associate Editor: Francesco Mazzarini

Received 19 June 2018
Revision received 25 October 2018
Accepted 8 February 2019

Published online 9 April 2019

Polyphase kinematic history of transpression along the Mecca Hills segment of the San Andreas fault, southern California

Steffen G. Bergh[1,*], Arthur G. Sylvester[2,*], Alula Damte[3,*], and Kjetil Indrevær[4,*]

[1]Department of Geosciences, University of Tromsø (UiT)–The Arctic University of Norway, N-9037 Tromsø, Norway
[2]Department of Earth Science, University of California, Santa Barbara, California 93106, USA
[3]Central European Petroleum Company, Ltd., Calgary, AB T2P 3T3, Canada
[4]Department of Geosciences, University of Oslo, 0371 Oslo, Norway

ABSTRACT

Miocene–Pliocene sedimentary rocks in the Mecca Hills, southern California, were uplifted and deformed by transpression along a restraining bend in the San Andreas fault trace between the Orocopia and San Bernardino Mountains in Pleistocene time. This paper presents field evidence for three stages of structural evolution of a complex, asymmetric wedge-like flower structure, expressed as: (1) subhorizontal en échelon folds and faults oblique to the San Andreas fault; (2) steeply plunging folds subparallel to the San Andreas fault; and (3) folds and thrust faults fully parallel to the San Andreas fault. We argue that the resulting flower-structure deformation formed successively from early distributed transpression through full (?) strain partitioning, rather than from active, synchronous, strike-slip–forming movements, as expected. The model is supported by crosscut relations of major folds and faults and strain estimates from minor conjugate shear fracture sets. The polyphase evolution initiated on a steep right-lateral strand of the San Andreas fault, producing thick fault gouge. Then, the adjacent Neogene strata were folded en échelon outward in a uniformly distributed simple shear strain field. The subsidiary Skeleton Canyon fault formed along a restraining bend that localized right-lateral shearing along this fault, and reshaped the en échelon folds into steeply plunging folds almost parallel to the San Andreas fault in a nascent partly partitioned strain field. The final kinematic stage generated SW-verging folds and thrust faults trending parallel to the San Andreas fault and decapitated the en échelon folds and faults. The switch from early, distributed strike-slip to late-stage regional slip-partitioned shortening (fold-thrust) deformation may have been locally induced by the bending geometry of the fault. The polyphase structures were active in successive order to balance the driving forces in one or more critical-angled transpressional and fold-and-thrust uplift wedges. Fault-related shortening, uplift, and erosion are still controlled in the Mecca Hills by combining and adjusting the wedges with low convergence angle, transpression, and lateral crustal motion in a San Andreas fault plate scenario. Our model, therefore, addresses a more nuanced view of a polyphase flower-structure system and highlights the need to more carefully sort out spatially and temporally different kinematic data as a basis for analog and numerical modeling of transpressional uplift areas.

INTRODUCTION

Many crustal-scale kinematic models have been proposed to explain strike-slip–dominated transpressional uplifts with flower-structure geometry (Harland, 1971; Wilcox et al., 1973; Sylvester, 1988) along the San Andreas fault in California (Mount and Suppe, 1987; Tikoff and Teyssier, 1994; Dewey et al., 1998; Schreurs and Colletta, 1998; Teyssier and Tikoff, 1998; Miller, 1998). Such uplifts are present along active restraining bends (Wakabayashi et al., 2004), and the kinematic behavior of the San Andreas fault has been explored using field data, earthquake studies, and analog and numerical models (e.g., Sylvester, 1988; Richard and Cobbold, 1990; Platt, 1993; Braun and Beaumont, 1995; Burbidge and Braun, 1998; Tavarnelli, 1998; McClay et al., 2004). Models of transpressional deformation vary from distributed simple shear (Sylvester, 1988) to combinations of localized simple shear and pure shear shortening (Figs. 1A, 1B), i.e., strain partitioning (Zoback et al., 1987; Mount and Suppe, 1987; Oldow et al., 1990). Formation of a symmetric transpressional flower-like uplift or wedge (cf. Leever et al., 2011a) requires ideal bulk simple shear (Fig. 1C), which is achieved by synchronous formation of distributed structures adjacent to a major strike-slip fault (cf. Sylvester, 1988). Most analog and numerical models, however, fail to match and cannot explain multiple branching, subparallel strike-slip and reverse faults, both along and across strike, and/or fault segmentation. Such complexities can be explained, however, by strain partitioning (Fig. 1), where strike-slip and shortening components are partly or fully separated (Oldow et al., 1990; Fossen and Tikoff, 1993; Fossen et al., 1994; Tikoff and Teyssier, 1994; Jones and Tanner, 1995; Miller, 1998; Tavarnelli, 1998; Tavarnelli and Pasqui, 2000; Holdsworth et al., 2002). The degrees of partitioning may result from changes in plate convergence angle, fault obliquity (Richard et al., 1991; McClay et al., 2004), and/or changing local strain fields (Mount and Suppe, 1987; Miller, 1998).

This study addressed the changing kinematics and strain fields, i.e., polyphase transpression and strain partitioning, in the Mecca Hills in Coachella Valley (Figs. 2 and 3), southern California. Nowhere else along its entire length are the San Andreas fault and its associated complex flower structures as well exposed for such study as they are in the Mecca Hills. From detailed field observations of uplifted and complexly deformed Miocene–Pliocene and

*E-mails: steffen.bergh@uit.no; sylvester@ucsb.edu; adamte@cepetro.com; kjetil.indrevar@geo.uio.no

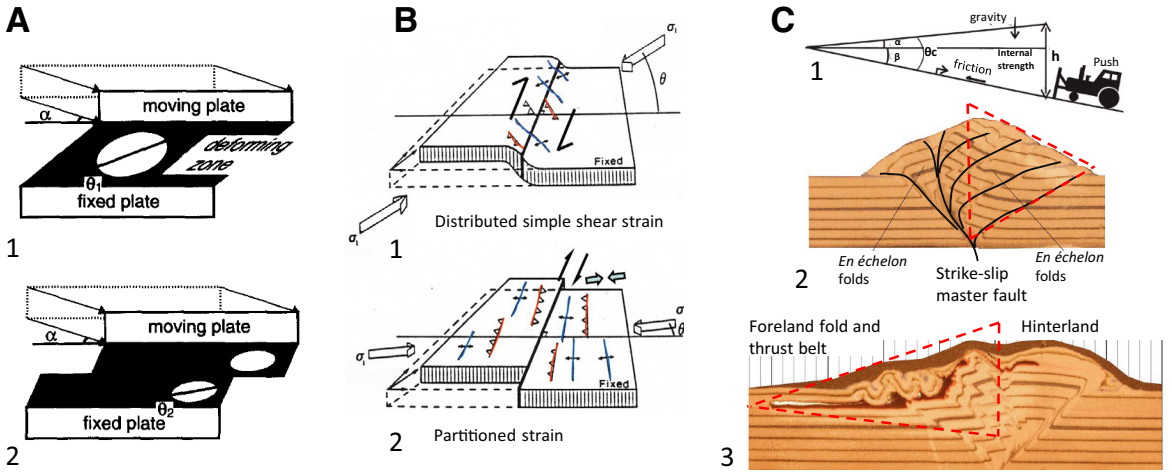

Figure 1. Contrasting transpressional deformation models and corresponding brittle wedges (flower structures), adapted from model results of transpression. (A) Sketch of two plates moving laterally with a convergence angle (α), resulting in distributed (1) and partitioned (2) deformation zones. Note that angle between shear zone and elongation direction of strain marker (θ) decreases with amount of partitioning (after Tikoff and Teyssier, 1994). (B) Distributed (1) and partitioned (2) shear deformation styles (fold and thrust) along a major dextral strike-slip fault. Note angle θ between contractile structures (perpendicular to the regional shortening direction) and fault is oblique, 30°–45° in distributed shear, whereas contractile structures (pure shear strain) and localized strike slip are almost parallel in full strain partitioning (Mount and Suppe, 1987). (C) Definitions of key variables of a Coulomb wedge (1) influenced by a push from behind (after Braathen et al.,1999), where wedge taper (θc and *h* = height) is the sum of surface slope (α) and the angle of basal faulting (β). (2) Experimental transpressional brittle wedge (flower structure) formed adjacent to a major strike-slip fault yielding oblique, distributed transpressional structures. (3) With long-term deformation and increased strain partitioning, the distributed uplifted wedge adjusts to a critical taper geometry by forming large-scale fold-and-thrust belt structures toward the frontal side of the wedge. Wedge taper is shown by red stippled lines. Figure is modified after Leever et al. (2011a, 2011b).

Pleistocene strata along the San Andreas fault, we argue that this relatively small range of hills may have formed in a temporally evolving transpressional system (cf. Sylvester and Smith, 1976, 1987; Sylvester, 1988) from distributed to partitioned strain events. The deformation affected an originally steep fault strand of the San Andreas fault and included en échelon folds and steep reverse faults oblique to the San Andreas fault (first stage), steeply plunging folds nearly parallel to the San Andreas fault (second stage), and folds and thrusts fully parallel to the San Andreas fault (third stage). These structures interacted with regional faults and folds outside the San Andreas fault (Fig. 3), such as the Painted Canyon fault, Skeleton Canyon fault, and Mecca anticline (Sylvester and Smith, 1976, 1987; Damte, 1997; McNabb et al., 2017). We analyzed the geometry, kinematics, and spatial-temporal relationships of the San Andreas fault–related structures in the field, including minor conjugate fracture sets, to record changes in transpressional and partitioned strain fields. Our hypothesis is that simple shear (transpressional) and pure shear (fold-thrust) uplift wedges formed successively (Fig. 1) to balance the internal forces in a crustal-scale critical taper (cf. Dahlen, 1990; Koons, 1994; Braathen et al., 1999). The results may be of broad interest and scientific significance, and they can be used to model distributed and partitioned strain fields in other restraining bend segments along the San Andreas fault (Teyssier and Tikoff, 1998; McClay and Bonora, 2001; Carena et al., 2004; Dolan et al., 2007; Dair and Cook, 2009; Cooke and Dair, 2011; Herbert and Cooke, 2012).

We used high-resolution (<10 m) digital elevation model (DEM) images accessed from Google Earth for detailed mapping, structural analysis, and investigation of relative timing of fold and fault structures, and to identify

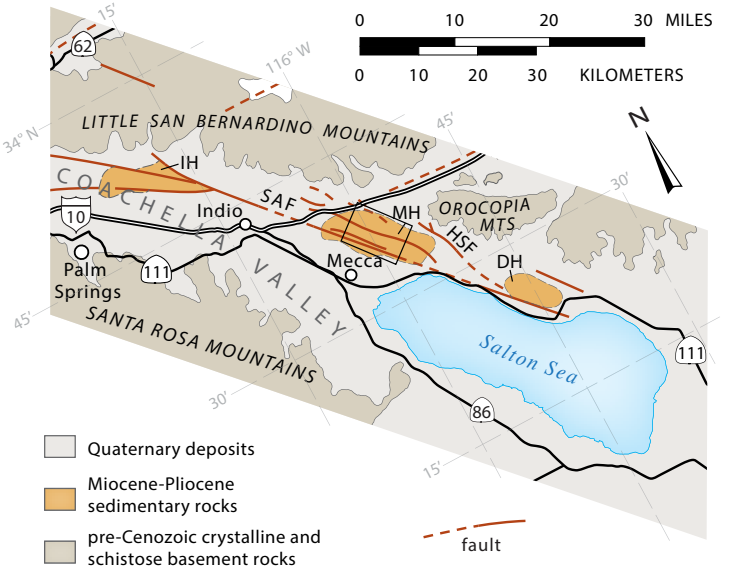

Figure 2. Geologic and simplified tectonic map of the San Andreas fault zone in Coachella Valley, Salton Trough, southern California. Note three main uplifted transpressional ridges, Indio Hills (IH), Mecca Hills (MH), and Durmid Hills (DH), and associated splay faults, including Hidden Spring fault (HSF). SAF—San Andreas fault. Frame locates Figure 3. Figure is modified from Sylvester and O'Black Gans (2016).

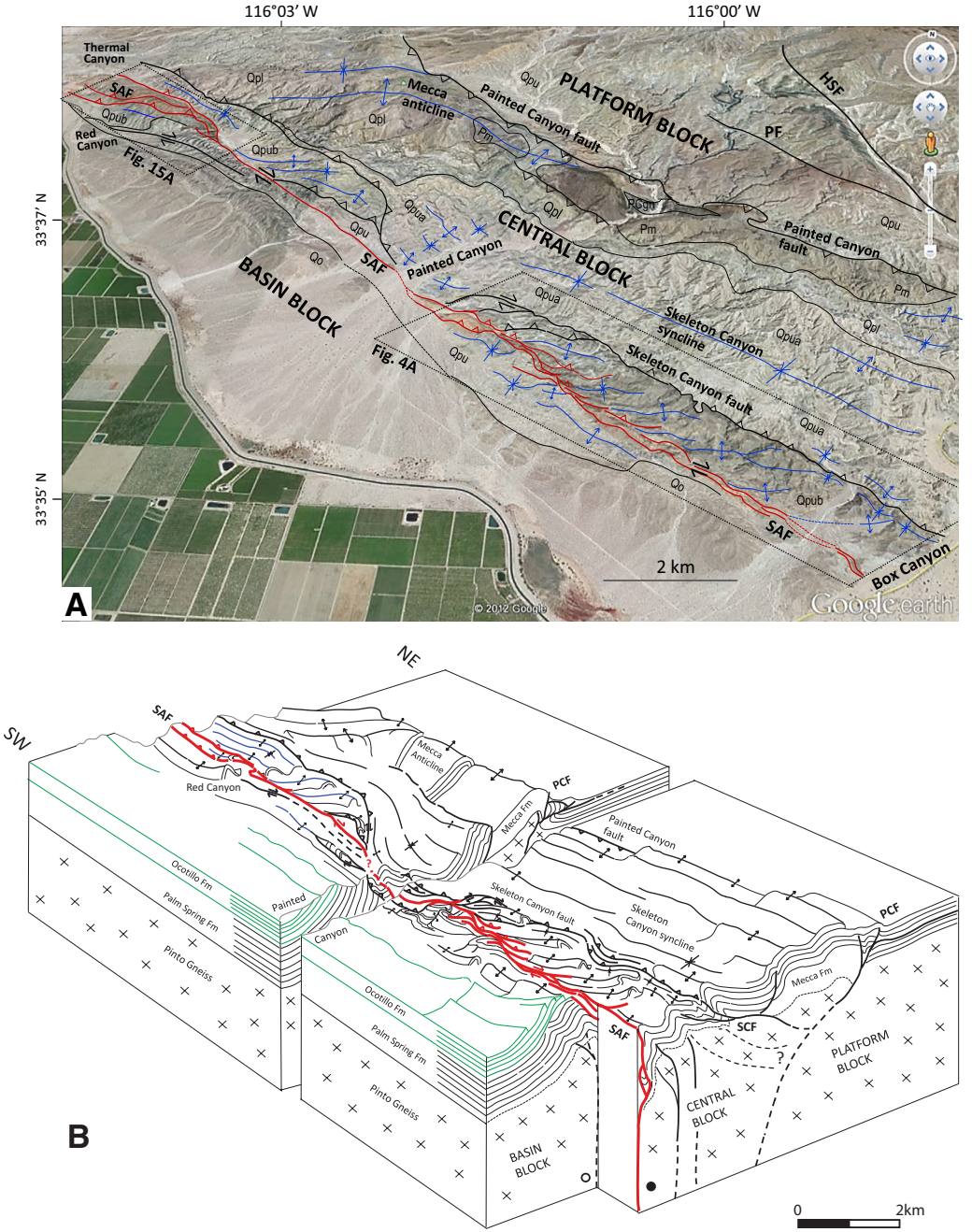

Figure 3. (A) Oblique Google Earth image of Mecca Hills area, taken in 2011, with major interpreted structures and (B) three-dimensional (3-D) sketch interpretation model. Both images illustrate large-scale structural architecture with three major crustal blocks, Basin block, Central block, and Platform block (Sylvester and Smith, 1976; 1987), and major faults, San Andreas fault (SAF), Skeleton Canyon fault (SCF), and Painted Canyon fault (PCF) and folds (blue lines in A), viewed toward north. Note irregular trace of San Andreas fault with alternating narrow and wide lens-shaped zones of fault gouge (in between red lines in A). Also note variable structural styles, both across strike and along strike, including oblique en échelon folds (red lines) and folds trending parallel to San Andreas fault (blue lines in A), e.g., Skeleton Canyon syncline and parts of Mecca anticline near Painted Canyon fault, and duplexes and step-over bends near Skeleton Canyon fault. The 3-D sketch model (Fig. 3B) is split into two NE-SW cross sections, one along Painted Canyon (center), and the other along Box Canyon (right). Stippled frames in A denote areas mapped in detail (Figs. 4A and 15A). Abbreviations: SAF—San Andreas fault, PF—Platform fault, HSF—Hidden Spring fault, Pcgn—Precambrian Pinto gneiss, Pm—Mecca Formation, Qpl—lower Palm Spring Formation, Qpu—Upper Palm Spring Formation, undifferentiated, Qpua—upper Palm Spring Formation, arkosic, Qpub—upper Palm Spring Formation, mudstone, Qo—Ocotillo Formation. Structural symbols are as in Figure 4A.

and trace stratigraphic units and fault gouge splaying outward from the San Andreas fault (Fig. 3A).

GEOLOGIC SETTING AND CENOZOIC TECTONIC HISTORY

The Mecca Hills are a NW-SE–trending, acute tectonic culmination in the Coachella Valley, southern California, bounded by the low-relief San Andreas fault segment and left-lateral splay faults between the Orocopia and San Bernardino Mountains (Fig. 2; Sylvester and Smith, 1976; Bilham and Williams, 1985; Spotila et al., 2007). This culmination is located along the northeast edge of the Salton Trough, which is a 5.5-km-thick Neogene sedimentary rift basin bounded on its southwest side by the major West Salton detachment fault (Dorsey et al., 2011) and on its northeast side by the San Andreas fault (Fig. 2). The Salton Trough is an active transform rift system marked by high heat flow, recent volcanism, and recurring seismicity (Dibblee, 1954, 1984; Hamilton, 1961; Hamilton and Myers, 1966; Robinson et al., 1976; Fuis and Kohler, 1984; Axen and Fletcher, 1998; Hulen and Pulka, 2001) at the northwest end of the Gulf of California. The trough formed by rifting of the proto–Gulf of California in Miocene time (ca. 12–8 Ma) linked with Basin and Range subsidence (Frost and Martin, 1982; Herzig and Jacobs, 1994; Axen and Fletcher, 1998; Shirvell et al., 2009; Dorsey et al., 2011). Initial displacement on the San Andreas fault in the Salton Trough started ca. 8–6 Ma, when it occupied an older Basin and Range normal fault along the evolving Pacific–North American plate margin (Frost and Martin, 1982; Herzig et al., 1988; Stock and Hodges, 1989; Winker and Kidwell, 1996; Atwater and Stock, 1998; Dorsey et al., 2011).

Parts of the Salton Trough basin underwent subsidence until ca. 1.2–1.0 Ma and were later uplifted, tilted, and variably deformed (Lutz et al., 2006; Dorsey et al., 2011). The Mecca Hills and corresponding Indio and Durmid Hills culminations (Fig. 2; Babcock, 1974; Keller et al., 1982; Bürgmann, 1991; Sylvester et al., 1993) record a history of synchronous basin subsidence, deposition, and early, right-lateral displacements along the San Andreas fault in the time period 4.0–1.0 Ma (Sylvester and Smith, 1976, 1987; Sylvester et al., 1993; Bilham and Williams, 1985; McNabb et al., 2017). The complex transform fault activity in the northeast part of the Salton Trough basin included transtensional subsidence and transpressional uplift of segmented domains in between localized strike-slip splay faults (Fig. 2). The uplift strongly affected Neogene strata of the Mecca Hills as well as underlying basement rocks (Sylvester and Smith, 1976; Crowell and Sylvester, 1979). Transpressional uplift occurred in the Mecca and Durmid Hills because of their location in a segment of the San Andreas fault that strikes more obliquely (15°) than elsewhere along San Andreas fault (<5°) relative to the regional plate-motion vector (Sylvester and Smith, 1976; Bilham and Williams, 1985). These segments produced local structures that accommodated small changes in the main trend of the San Andreas fault (Saucier et al., 1992).

Prevailing models for slip rates on the San Andreas fault in central California indicate an average of 39 ± 2 mm/yr (Argus and Gordon, 2001), whereas slip rates estimated for right-lateral strike-slip faults in the western Salton Trough since 1.07 Ma are lower, in the range of 20.1 +6.4/–9.8 mm/yr to 5.4 +5.9/–1.4 mm/yr (Janecke et al., 2010). The decrease in slip rates through time may be due to a possible structural readjustment after ca. 0.6–0.5 Ma, where right-lateral movement was transferred to other, nearby faults (Janecke et al., 2010). In the Salton Trough basin, a minimum of 160 km and maximum 300 km of dextral lateral translation are suggested since the fault entered the Salton Trough 6 m.y. ago (Crowell, 1981; Matti and Morton, 1993; Nicholson et al., 1994; Ingersoll and Rumelhart, 1999; Oskin and Stock, 2003; Dorsey et al., 2011). These displacement estimates are consistent with an average modeled lateral slip rate of 20 mm/yr (Fattaruso et al., 2014) and ~3.7 mm/yr of shortening accommodated by the Mecca Hills since the onset of transpression (Sieh and Jahns, 1984). The shortening estimates, however, are much higher than for other segments in the San Andreas fault system, such as the Rinconada fault system in northern California, where shortening rates of only 0.3–1.1 mm/yr are obtained (Titus et al., 2007).

STRATIGRAPHY OF THE MECCA HILLS

About 2–3 km of Pliocene–Pleistocene nonmarine, lacustrine, fluvial/braided stream, and alluvial-fan delta deposits accumulated in several subbasins in the Salton Trough, including Mecca basin (Damte and Biehler, 1995; Damte, 1997; McNabb et al., 2017). Stratigraphic and paleomagnetic reversal data (McNabb et al., 2017) suggest that deposition in Mecca basin was prolonged and more complex than proposed earlier (Dibblee, 1954; Sylvester and Smith, 1976); nonetheless, we retain herein the previously published stratigraphy for Mecca basin rather than adapt stratigraphy schemes from other parts of the Salton Trough.

The Mecca Hills (Fig. 3) expose the late Proterozoic Pinto Gneiss, which was intruded by Mesozoic granite and Cenozoic rhyolite, and which is overlain by a ≤1.6-km-thick succession of late Miocene (?) to Pliocene and Pleistocene lacustrine and fluvial deposits, and late Pleistocene and Quaternary alluvium (<100 m thick). The lowest sedimentary succession is the late Miocene Mecca Formation, consisting of locally derived debris-flow and alluvial-fan conglomerate. The Mecca Formation is overlain by the Pliocene Palm Spring Formation, which consists of a lower member of interbedded, fluvial and lacustrine, pebbly sandstone and siltstone and an upper member of pebbly arkosic sandstone and lacustrine mudstone. These fluvial and lacustrine deposits are capped by late Pleistocene to Quaternary (0.76 Ma) Ocotillo Formation fanglomerate (Dibblee, 1954; Sylvester and Smith, 1976, 1987; Boley et al., 1994; Sheridan and Weldon, 1994; Winker and Kidwell, 1996; McNabb et al., 2017). The exact age of the Mecca Formation is not known due to lack of age-diagnostic fossils. Reversed magnetic polarity dating of the Palm Spring Formation (Chang et al., 1987; Boley et al., 1994) and accumulation rates below the 0.765 Ma Bishop Tuff (Zeeden et al., 2014) in the uppermost succession, however, yield dates of ca. 3.7–2.6 Ma for its lower member and ca. 2.8–0.76 Ma for its upper member (McNabb et al., 2017). A prominent unconformity between the lower and upper members of the Palm Spring Formation (Sylvester and Smith, 1976; Damte

and Biehler, 1995; Damte, 1997; McNabb et al., 2017) marks the onset of localized transtensional deformation ca. 3.0–2.4 Ma in the Mecca Hills (McNabb et al., 2017). The sedimentary deposits were derived from uplifted sources northeast of the San Andreas fault, transported southeastward along strike of active parts of the San Andreas fault, and deposited as alluvial fans and riverbed material surrounding smaller, fault-bounded lake deposits (Dibblee, 1954; Sylvester and Smith, 1976; Damte, 1997; McNabb et al., 2017) in a widening Salton Trough basin.

In early to mid-Pleistocene time (ca. 2.2–0.76 Ma), the Mecca basin and adjacent basin-bounding normal faults inverted, so that Miocene–Pliocene strata were deformed and uplifted by transpression along the San Andreas fault. Initial inversion of the basin may have started as early as the mid-Pliocene (3.0–2.4 Ma), as indicated by the angular unconformity in the Palm Spring Formation, paleomagnetic reversals at this time interval, changing subsidence rates, and abrupt thickness changes of the Mecca and Palm Spring Formations across San Andreas fault and adjacent faults (Sylvester and Smith, 1976, 1987; McNabb et al., 2017). A critical feature for absolute timing of the transpressional uplift deformation outlined in this work is the presence of the 0.765 Ma Bishop Tuff (Zeeden et al., 2014) in the uppermost upper member of the Palm Spring Formation, where it underlies the Ocotillo Formation in the Central block near Thermal Canyon (McNabb et al., 2017).

MAJOR STRUCTURE OF THE MECCA HILLS

The Mecca Hills may be separated into three structural blocks: The Basin block southwest of the San Andreas fault, the Central block between the San Andreas and Painted Canyon faults, and the Platform block northeast of the Painted Canyon fault (Fig. 3; Sylvester and Smith, 1976, 1987). These blocks were affected by contrasting styles of deformation during inversion of the Mecca basin. The Basin block exposes only upper Palm Spring Formation strata and overlying Ocotillo Formation (Fig. 3). The Palm Spring strata are intensely folded and faulted along the southwest side of the San Andreas fault and change structural styles both across and along strike. The Ocotillo Formation is merely tilted basinward southwest of the San Andreas fault, and its contact with the underlying Palm Spring Formation is mostly an angular unconformity (Fig. 3).

In the Central block, a major fold set (Mecca anticline and related syncline) trends on average 30° counterclockwise (WNW-ESE) from the San Andreas fault in the north near Thermal Canyon, but it bends parallel to the Painted Canyon fault and San Andreas fault (NW-SE) in the south (Fig. 3). The Mecca anticline plunges gently NW from its core of uplifted basement rocks in Painted Canyon, where the Mecca Formation overlies basement rocks in a buttress unconformity. The Skeleton Canyon syncline, a broad, San Andreas fault–parallel (NW-SE–trending), upright syncline, folds the entire Miocene–Pliocene succession but dies out northwestward (Fig. 3). The southwest flank of the syncline is cut by the moderately NE-dipping Skeleton Canyon fault, interpreted as a thrust ramp underlying the Skeleton Canyon syncline (Sylvester and Smith, 1976, 1987). The Skeleton Canyon fault obliquely truncates E-W–trending en échelon folds where it approaches the Basin block, but near the mouth of Painted Canyon, it merges into the San Andreas fault (Fig. 3).

The northeast boundary between the Central block and the largely undeformed Platform block is marked by the Painted Canyon fault (Fig. 3), a steep, SW-dipping, oblique reverse strike-slip fault (Sylvester and Smith, 1976). The junction between the Central and Platform blocks in Painted Canyon is a complex triangle zone in which strata are cut by low-angle thrust faults that propagated into horizontal strata and emplaced steep, overturned strata northeastward upon nearly horizontal units in the Platform block (Sylvester and Smith, 1976, 1987).

For this field study, we mapped and analyzed the San Andreas fault and adjacent structures of two areas in the Basin and Central blocks (Fig. 3): a 5-km-long zone between Box and Painted Canyons (Fig. 4A), and a 2-km-long zone in the northwest near Thermal Canyon (Fig. 3A).

SAN ANDREAS FAULT CORE

The San Andreas fault trace has an irregular, step-wise and anastomosing geometry in the Mecca Hills with subsidiary fold and fault strands striking both oblique to (WNW-ESE) and parallel to (NW-SE) the San Andreas fault (Figs. 3 and 4). The main San Andreas fault core zone consists of a distinct and poorly consolidated, red-brown fault gouge/breccia with random sandstone clasts and up to half-meter–sized, subrounded sandstone blocks, termed phacoids, which are embedded in a red-brown–stained clay to silty matrix (Fig. 5A). A closely spaced schistose fabric is present near San Andreas fault core contacts, not in the interior of the core as expected (cf. Rowe and Griffith, 2015). This fabric splays outward into steep lateral faults containing subhorizontal slickensides and minor kink folds (Fig. 5B).

The core zone of San Andreas fault gouge varies in shape and width, from narrow, linear zones less than 10 m wide near the fault core, via en échelon and step-wise lenses oblique to the San Andreas fault, to very wide zones (200–500 m) mostly parallel to the San Andreas fault (Figs. 3, 4, and 5C–5F). Similarly, deformation structures in surrounding Palm Spring strata display distinct styles and geometric complexities, e.g., variable fold axis plunge, and dip of faults and fold axial surfaces (Fig. 6A).

POLYPHASE STRUCTURAL ASSOCIATIONS IN MECCA HILLS

Three distinct fold and fault associations were mapped along the San Andreas fault and adjacent areas of the Basin and Central blocks: (1) oblique subhorizontal en échelon folds and steep reverse faults, (2) steeply plunging (subvertical) folds and steep lateral faults, and (3) folds and gently dipping thrust faults fully parallel to the San Andreas fault. Next, we describe and argue for a three-stage temporal evolution of such structures in Palm Spring strata

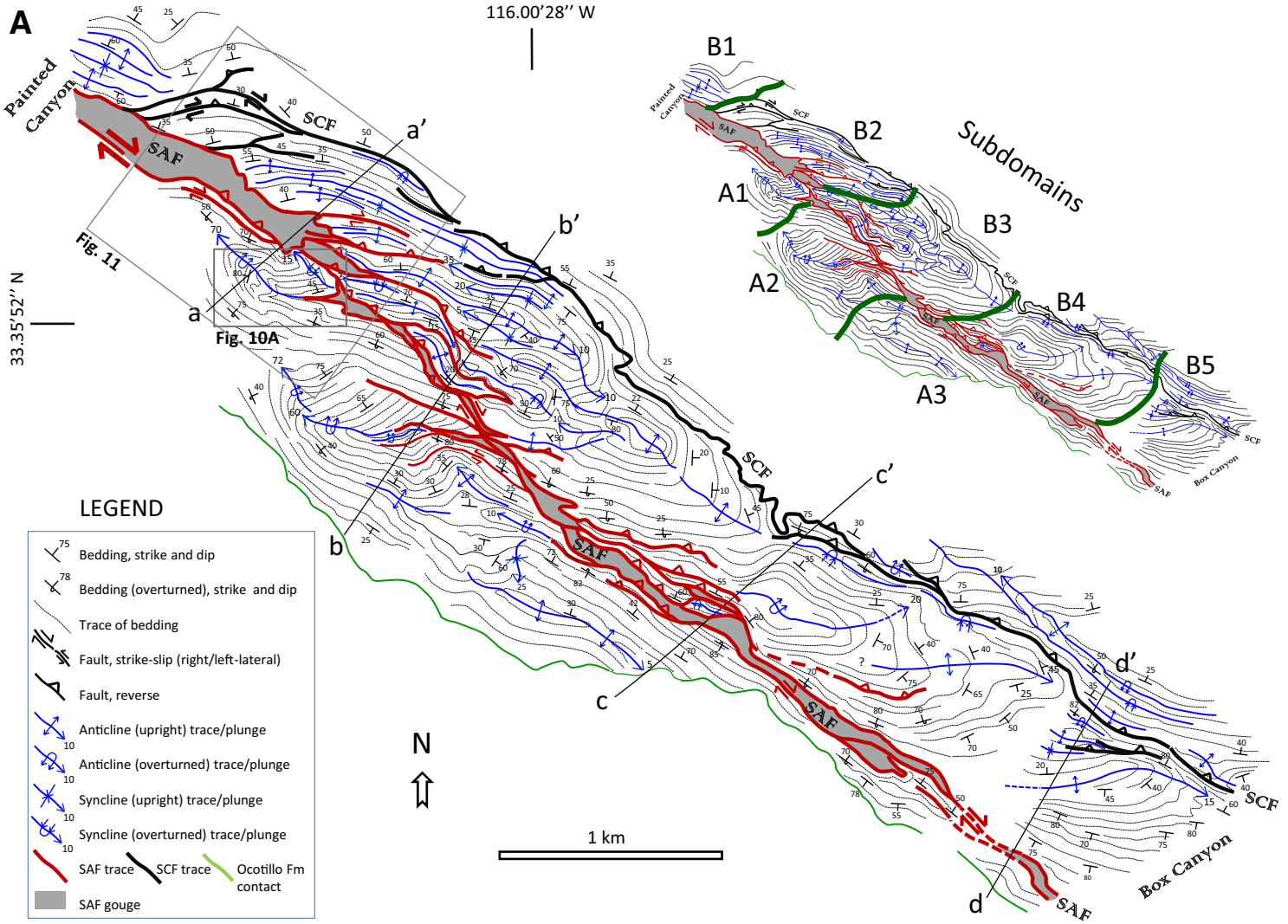

Figure 4. (A) Detailed structural map of area along San Andreas fault between Box and Painted Canyons (see location, latitude/longitude in Fig. 3) showing outline geometry of San Andreas fault (SAF), its fault gouge core zone, and adjacent areas of Basin and Central blocks, including Skeleton Canyon fault (SCF). Note irregular shape and variable width of San Andreas fault gouge, complex traces of en échelon folds, steeply plunging folds in Basin block, San Andreas fault–parallel folds and faults, and direct stepover linkage of San Andreas fault and Skeleton Canyon faults in northwestern part near mouth of Painted Canyon. Traces of bedding are marked as full (certain) and stippled (uncertain) lines. San Andreas fault gouge zone is shaded gray, and San Andreas fault contacts are shown as heavy red lines. Lines a-a' to d-d' locate cross sections in part B. Index map, upper right, depicts various subdomains (A1–A3, B1–B5) referred to in text. (*Continued on following page.*)

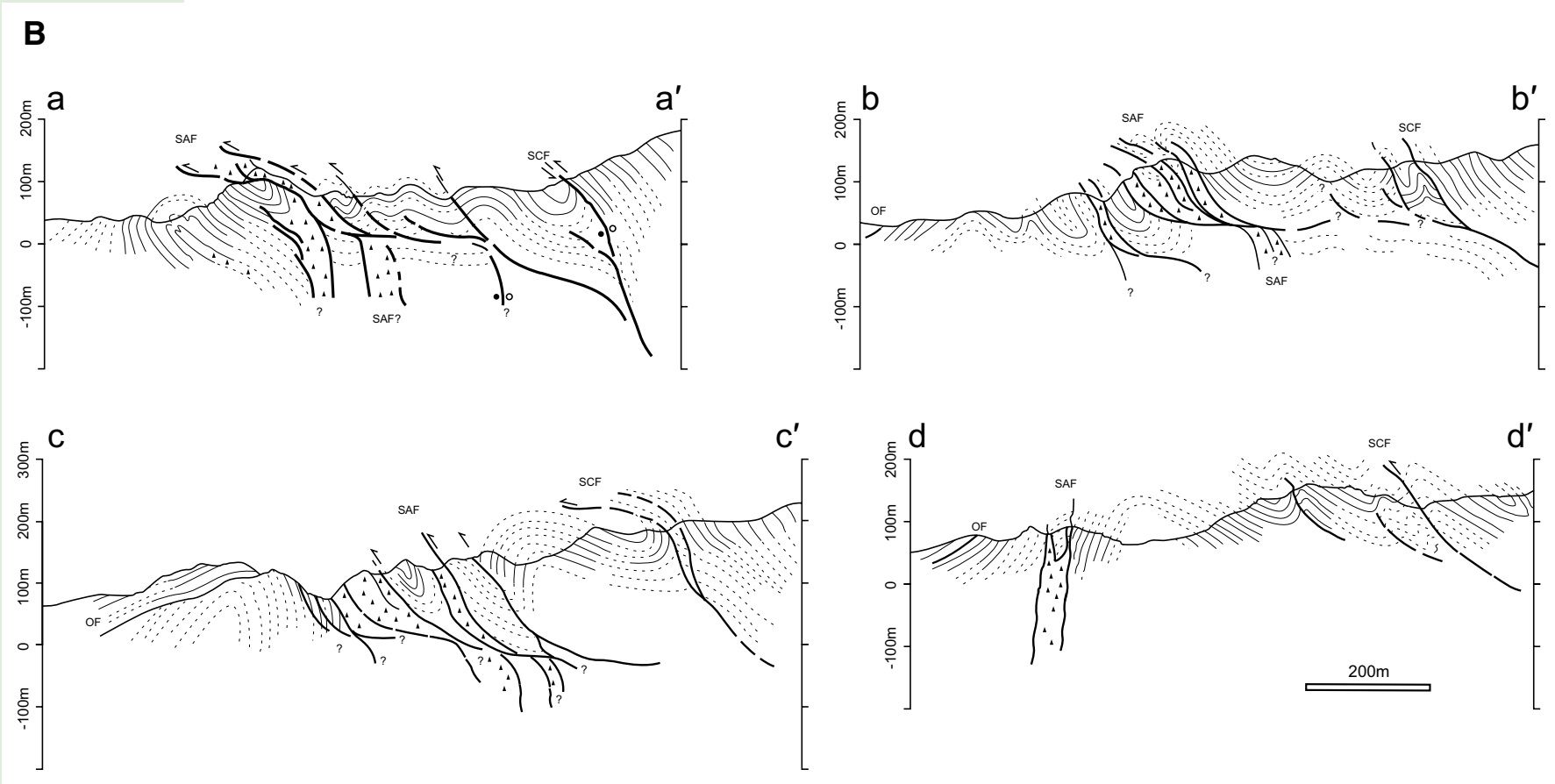

Figure 4 (*continued*). (B) Interpreted structural cross sections from the mapped area along San Andreas fault (see location of lines in part A). Traces of bedding are marked as full (certain) and stippled (uncertain) lines. San Andreas fault gouge is shown by black triangles. Abbreviations: SAF—San Andreas fault, SCF—Skeleton Canyon fault, OF—Ocotillo Formation.

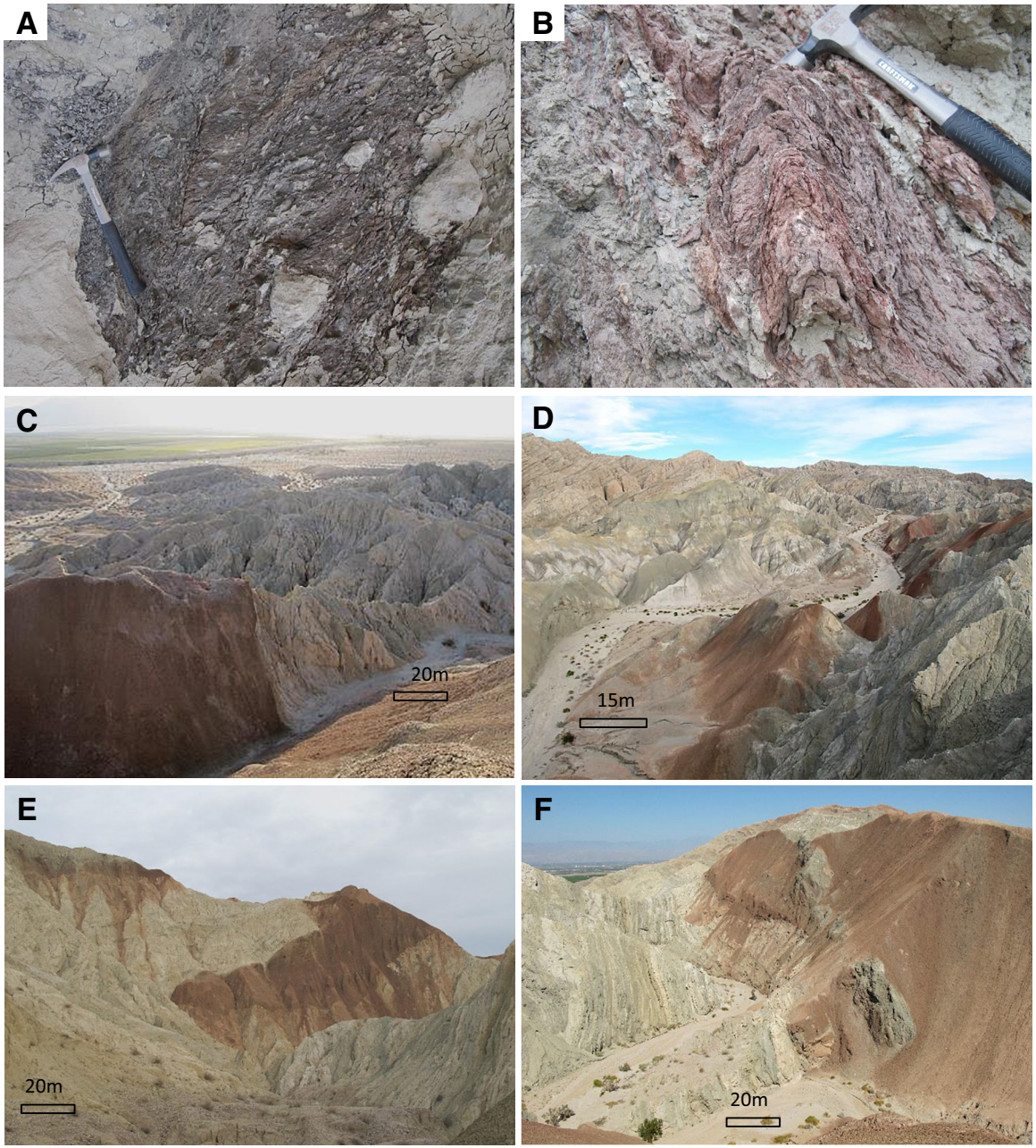

Figure 5. Outcrop photos of large-scale and internal characters of San Andreas fault red-brown–stained fault gouge zones in various areas of Mecca Hills. (A) Fault gouge in subdomain B2 with random sandstone clasts and blocks (phacoids) embedded in clay to silty matrix. (B) Internally folded, schistose fabric in San Andreas fault gouge. Locality: Red Canyon. (C) Steep, sharp contact between red-brown–stained San Andreas fault gouge and NE-dipping strata of Palm Spring Formation, in subdomain A2 of Basin block, view south. (D) San Andreas fault gouge zones arranged en échelon and inside hinges of oblique en échelon folds in Central block, subdomain B2. View east. (E) Gently dipping to subhorizontal San Andreas fault gouge zones at Red Canyon, repeated by SW-directed thrust fault. Lower gouge zone is in hinge of recumbent, isoclinal fold (see Figs. 15C and 16C). View ESE. (F) Part of an up to 500-m-wide San Andreas fault gouge zone at Red Canyon repeated by thrust slices with internal remnants of Palm Spring host-rock strata. Note ramp-flat geometry of thrust and emplacement of gouge over steeply dipping (folded) Palm Spring strata. See cross section in Figure 15C for interpretation. View NW.

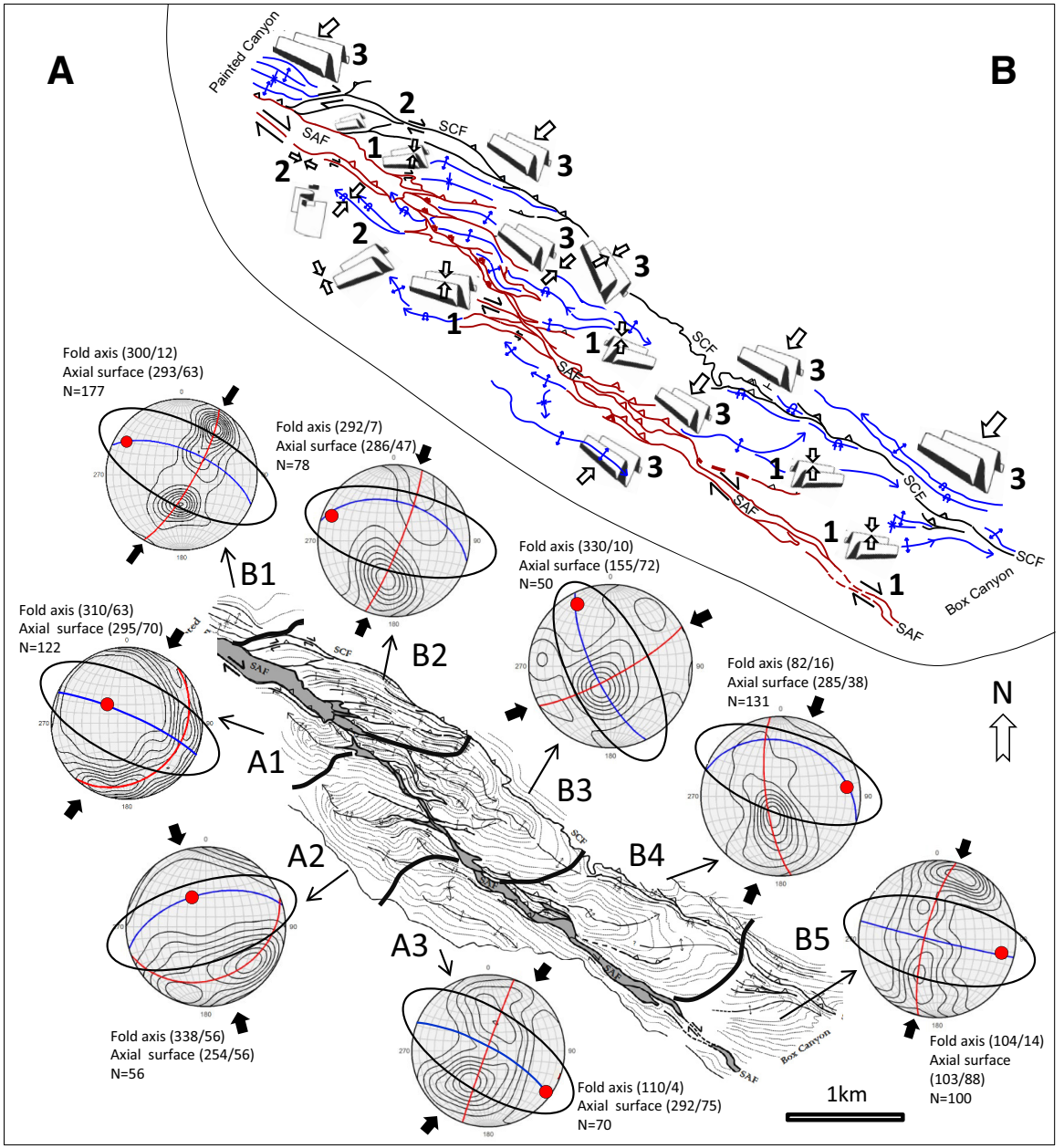

Figure 6. (A) Structural orientation data and interpreted local strain fields (two-dimensional strain ellipses) based on fold orientation data in study area. Lower-hemisphere Schmidt stereograms of contoured poles to bedding and average fold girdle (red), average fold axes (red dots), and axial surfaces (blue great circles) in folded Palm Spring Formation strata from subdomains on either side of San Andreas fault. Subdomains are outlined as in Fig. 4A. Interpreted local strain fields (*x-z* axes of strain ellipse) for each subdomain are outlined as black ovals; heavy black arrows designate local shortening directions inferred from average fold orientations. Note change in strain field characteristics and shortening directions both along strike and across strike. Individual subdomains display specific structural geometries and kinematic characters, as apparent from San Andreas fault–oblique en échelon folds (in B2–B5), steeply plunging en échelon folds, and San Andreas fault–parallel strike-slip faults (in A1–A2), and San Andreas fault–parallel folds and thrust faults (in B1, B2, and A3). (B) Map summarizing spatial and temporal evolution of structures during the three kinematic stages (numbered as steps 1–3) based on fold and fault associations, kinematic data, and shear fracture orientation in the Mecca Hills segment of San Andreas fault (see Fig. 4A). Local shortening and sense of shear directions (arrows and half-arrows) are indicated for different subdomains. Note how changes in attitude of San Andreas fault trace correspond with fold and fault associations. Abbreviations: SAF—San Andreas fault, SCF—Skeleton Canyon fault.

adjacent to the San Andreas fault core zone (Fig. 5), based on crosscutting and overprinting relationships (Fig. 6B).

En Échelon Folds and Faults Oblique to the San Andreas Fault

Upright and gently plunging (<15°), WNW-ESE–trending en échelon folds and steep, NNE-dipping reverse faults are the most common fold and fault association in upper Palm Spring strata in subdomains B2 and B3 of the Central block (Figs. 3, 4A, and 6). Their average trend is 25°–40° clockwise to the NW-SE strike of the San Andreas fault, and they branch and widen obliquely outward from the steep San Andreas fault gouge zone and affect the upper Palm Spring strata up to 1 km away from the gouge (Figs. 4A, 5D, and 5E). In map view, en échelon fold hinges, traces of axial surfaces, and faults merge and make variable left bends with both low (<25°) and high (>40°) obliquity angles relative to San Andreas fault trace (Figs. 4A and 6; subdomains B2 and B3). These changes in fold trends are interpreted as small stepovers that correspond with changes in strike of the main San Andreas fault gouge boundary (Fig. 4A). Such geometric characteristics match well with transpressional folding in general (Jamison, 1991; Titus et al., 2007).

In cross section, en échelon folds define open anticline-syncline pairs that are variably asymmetric, locally with steep beds dipping south (Fig. 4B; cross sections a-a′, b-b′), and gently plunging fold axes (5°–15°) both away from (ESE) and toward the San Andreas fault (WNW; Fig. 6). The fold geometry varies from concentric in sandstone beds to tight upright folds in mudstones, producing doubly verging, symmetric fold patterns. More complex, asymmetric (SW-verging) and disharmonic parasitic folds are present in limbs and fold hinges (Figs. 7A–7C) close to the Skeleton Canyon fault (Fig. 4B, cross-section b-b′).

In subdomains B4 and B5 near the Skeleton Canyon fault, the axial traces of en échelon fold hinges bend clockwise into parallelism with the NW-SE fault trace (Fig. 4A). Similar changes in fold axial traces are shown by en échelon folds close to the San Andreas fault core (subdomain B2), and along irregular San Andreas fault fold traces in the Basin block (subdomains A1 and A2), where the obliquity (θ) varies from 45° to 0° due to local bending into complete parallelism with the San Andreas fault (see below).

En échelon faults (lateral and reverse) in map view branch outward from the San Andreas fault core into Palm Spring strata of the Central and Basin blocks and generally either follow the trace of the hinge and/or cut across limbs of asymmetric en échelon folds (Fig. 4A). Most splay faults have red-brown gouge cores that commonly end blindly within tightened fold hinges (Figs. 4A, 5D, 7D, and 8). In map view, these faults and associated gouge zones have curvilinear traces, mostly WNW-ESE strikes, and moderate dips to the north, with a right-stepping character accompanied by smaller-scale restraining bends, duplexes, and transfer zones (Fig. 4A). Individual faults are steep strike-slip faults close to the San Andreas fault trace, becoming shallowly N-dipping and reverse at increasing distance from the San Andreas fault (Fig. 4). The most pronounced is the Skeleton Canyon fault (Dibblee, 1954; Sylvester and Smith, 1976), which represents a single en échelon fault in the area where it splays out from the San Andreas fault at the B1-B2 boundary (Fig. 4A). For most of its length southeastward from subdomain B2 to B5, however, the Skeleton Canyon fault is subparallel to the San Andreas fault and slightly truncates the en échelon folds (Figs. 3, 4A, and 7).

Steeply Plunging Folds and Faults Parallel to the San Andreas Fault

Upright en échelon folds are also present in the Basin block, where they splay westward from the San Andreas fault core, making an angle of ~45° to the San Andreas fault trace (Figs. 4A and 8). In contrast to those of the Central block, however, these folds gradually change trend and plunge away from the San Andreas fault to a point where their plunge is nearly vertical (Fig. 9; Hamilton and Myers, 1966), and their axial traces become subparallel to the San Andreas fault trace (Figs. 4A, 6, and 10A; in subdomains A1 and A2). These geometric changes suggest that the steep and gently plunging folds are part of the same fold system, but that the steeply plunging folds are younger. A younger age is supported by a second set of large-scale folds that caused refolding of the en échelon fold traces (Fig. 11), although such folds have not yet been mapped and studied in detail (see Discussion). Notably, the southern limbs of the refolded folds appear to be overlapped by Ocotillo Formation strata, which provide an important time marker (see below).

Details of the complex geometric change (refolding) of gently plunging en échelon folds into steeply plunging folds are observed in subdomains A1 and A2 (Figs. 10 and 11). Where tight, W-E–trending en échelon folds splay out from the San Andreas fault at a moderate map angle (40°), they make an abrupt right bend that results in a second, NW-SE axial trace subparallel to San Andreas fault, and a corresponding change to steeply plunging fold axes (60°–72°). In the bent fold hinge (Figs. 9–11), small-scale, tight to isoclinal, locally disharmonic, subvertical shear folds with thickened, inclined, and partly overturned limbs, and narrow (<10 m) bed/limb-truncating strike-slip fault zones are present. These geometric changes caused repetition and complex modification of Palm Spring strata in subdomains A1–A3 (Figs. 3 and 4A).

Similar attitudinal changes in en échelon fault geometries are also observed. For example, the Skeleton Canyon fault splays out southeastward obliquely from the San Andreas fault in subdomain B2 of the Central block near Painted Canyon (Fig. 4A), where it makes a gradual left bend and splits into several dextral-oblique reverse and strike-slip fault duplexes (cf. Woodcock and Fischer, 1986). Southeastward, the fault strike changes from oblique to the San Andreas fault (45°) to fully parallel with the San Andreas fault in subdomain B5. Here, the Skeleton Canyon fault merges into the core of the underlying, NW-SE–trending Skeleton Canyon syncline, which makes up a large part of the Central block (Fig. 3).

In subdomains A1 and A2 of the Basin block, en échelon folds splaying outward from the San Andreas fault are associated with steeply dipping faults with meter-wide zones of red-stained gouge (Fig. 8). Such faults are

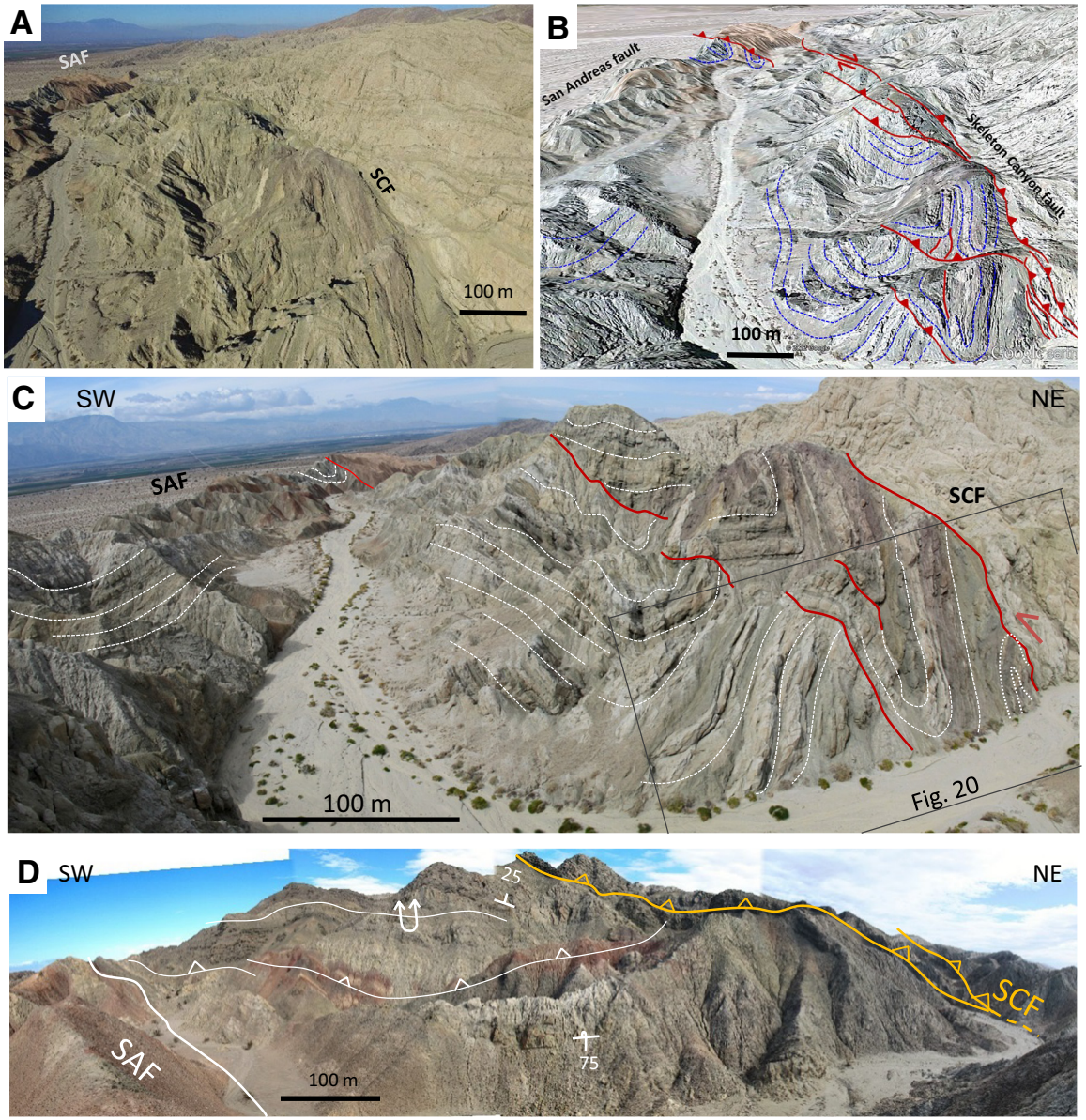

Figure 7. (A) Outcrop aerial view toward northwest of Skeleton Canyon fault (SCF) and adjacent Palm Spring strata in its footwall and hanging wall in subdomains B2 and B3 along Central block (see Fig. 4A for location). San Andreas fault is in background. Photo was taken from ~100 m above canyon floor. (B) Digital elevation model (DEM) image (Google Earth) of same area as in A, with interpreted fold and fault structures and relation to San Andreas fault. Note how Skeleton Canyon fault merges into and links up with San Andreas fault and obliquely truncates en échelon folds and reverse faults in footwall. Similarly, en échelon fold styles change where approaching Skeleton Canyon fault, from open and upright away from fault (left side of valley) into tight, partly disharmonic styles close to fault. En échelon folds are cut and overridden by thrust faults splaying from Skeleton Canyon fault. These faults also override San Andreas fault (at distance). (C) Panorama outcrop view of same fold and fault system as in A and B. (D) Outline photograph of a major en échelon fold and fault system in subdomain B4, having Palm Spring fold limb strata overturned to the south. Hinge-related reverse faults with internal gouge (red-brown) splay from San Andreas fault (SAF) and end blindly in hinge of large-scale en échelon fold. Fold is overridden by the Skeleton Canyon fault (SCF; to right in photo).

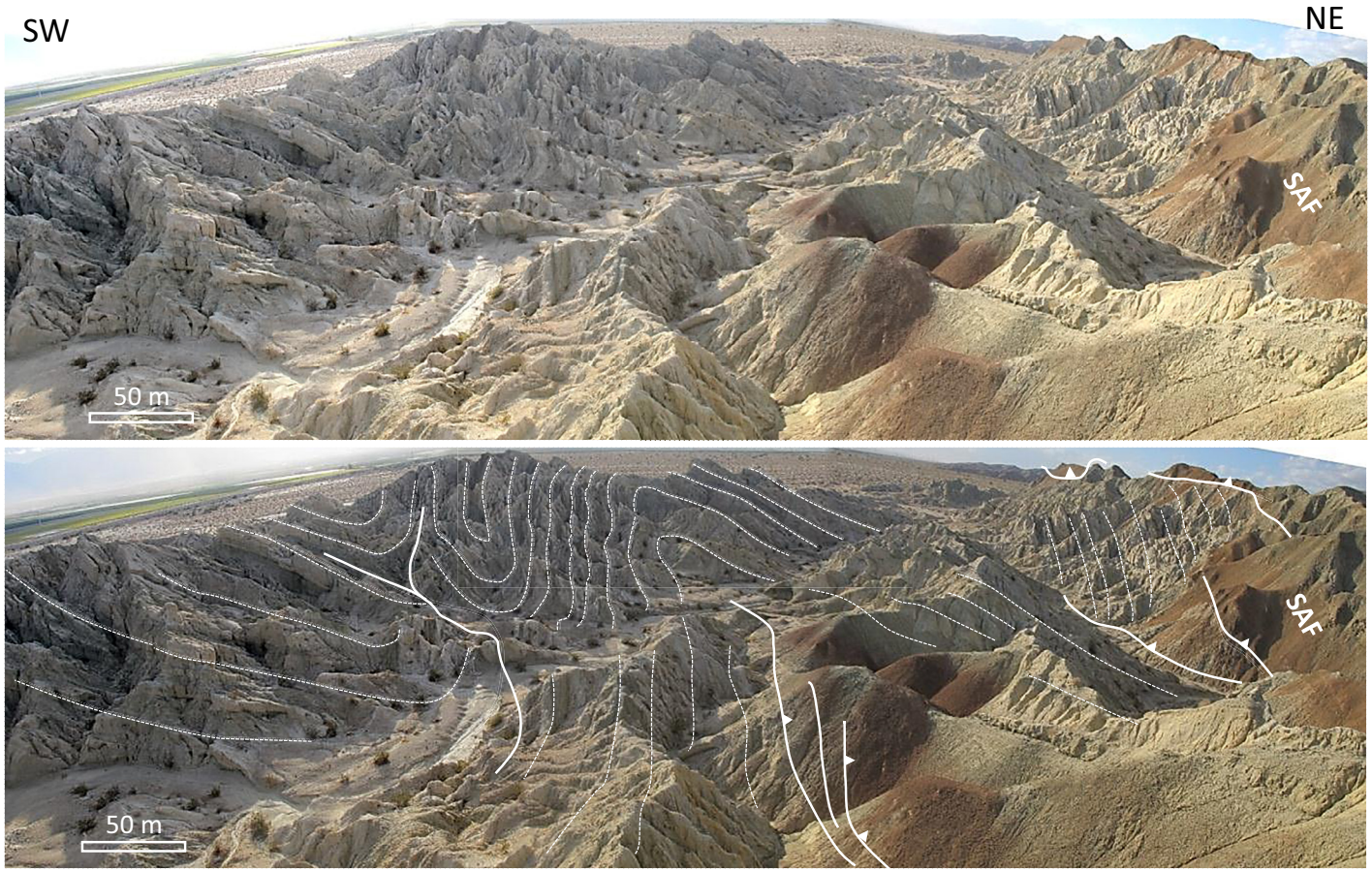

Figure 8. Overview photo (above) and interpretation (below) of a large-scale, steeply plunging en échelon fold system splaying from the San Andreas fault (SAF) in the Basin block of subdomain A (for location see Fig. 4A), on the southwest side of the San Andreas fault. Note presence of red-brown gouge zones inside imbricate, subvertical reverse faults, ending blind within the fold hinge. Trace of main San Andreas fault is on right in photo.

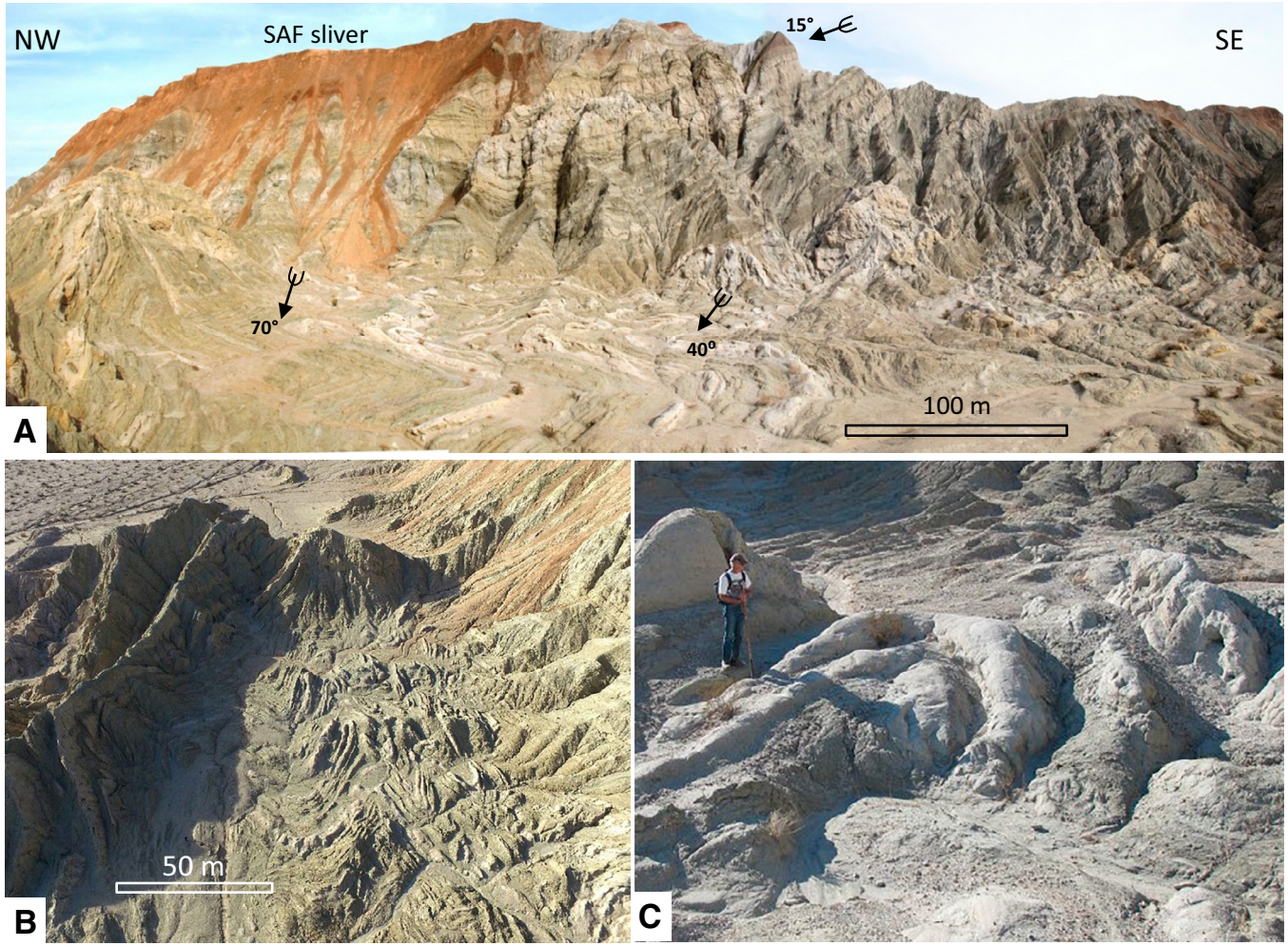

Figure 9. (A) Steeply plunging folds in subdomain A1 of Basin block (for location see Fig. 4A). Trace of San Andreas fault (SAF) is red-brown–stained gouge in thrust sliver along crest of the ridge. San Andreas fault–oblique Palm Spring strata in hillside are bent into parallelism with San Andreas fault and make a complex large-scale fold with subsidiary, parasitic small-scale folds (see map in Fig. 4A; see also Fig. 11). San Andreas fault contact is subhorizontal and marked by a younger thrust overriding the steep folds (see Figs. 10A and 12A). (B) Nearly down-plunge NW-ward view of same large-scale subvertical fold system as in A, taken from ~120 m above valley floor. Note tight and attenuated fold limbs parallel to San Andreas fault (off photo to the right) and fold axial surfaces. (C) Detail of small-scale, subvertical, concentric-shaped fold in competent Palm Spring sandstone bed. View is WNW.

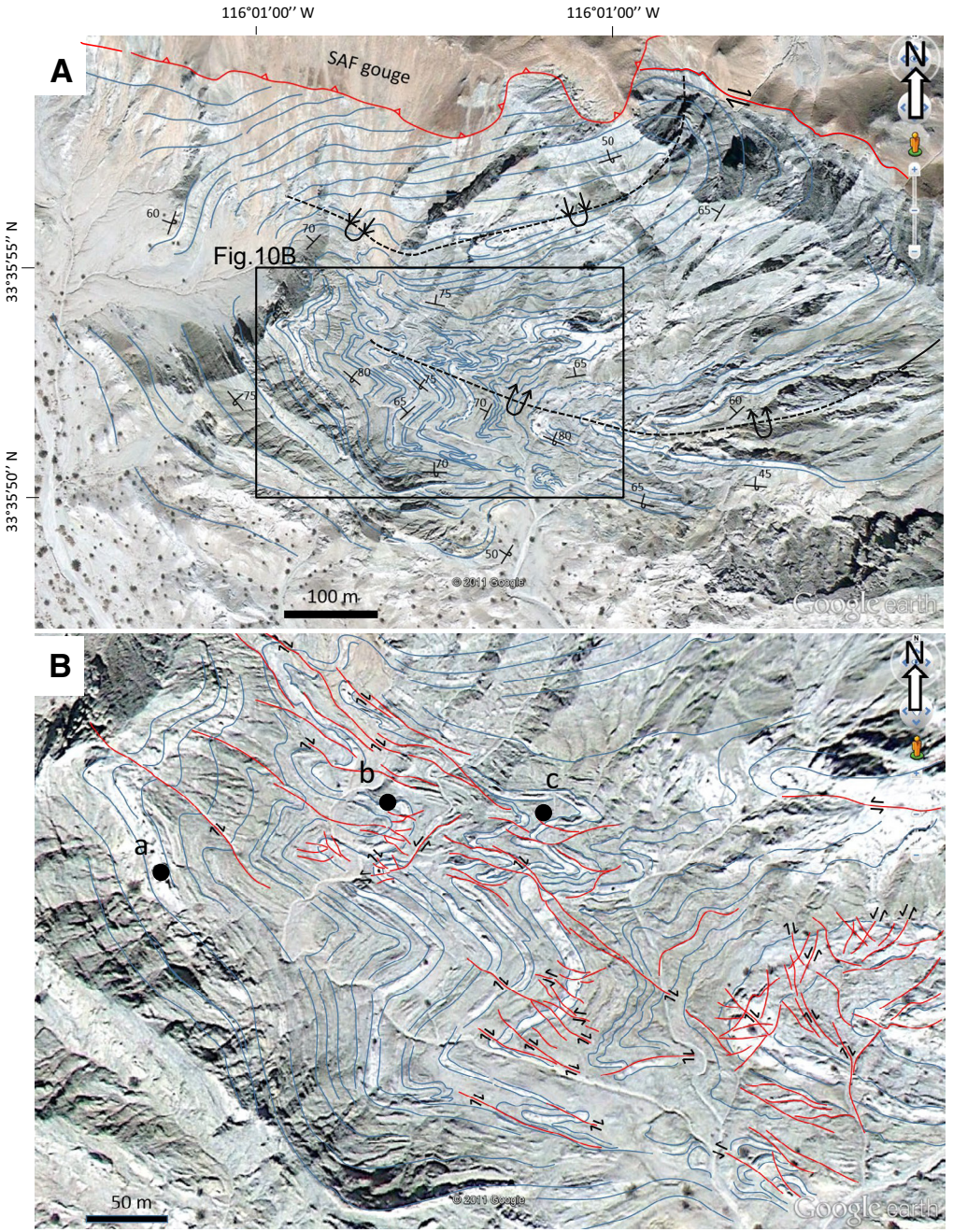

Figure 10. Google Earth image map of large-scale and smaller-scale (parasitic), steeply plunging en échelon folds realigned into parallelism with San Andreas fault (SAF) in subdomain A1 (for location see Fig. 4A). Note change in axial trends (stippled black lines) from San Andreas fault–oblique (right) to San Andreas fault–parallel fold trends (left of center) and corresponding change from symmetric, tight concentric to strongly appressed, similar fold styles, indicating lateral shearing parallel to axial surface (i.e., San Andreas fault). Note subhorizontal thrust below sliver of San Andreas fault gouge (top part of map) truncating steeply plunging folds, i.e., an out-of-sequence thrust. (B) Details from hinge zone of large-scale fold system in part A, showing complex geometric styles of steeply plunging folds, hinges, tightened limbs, and presence of steep, axial-planar right-and left-lateral strike-slip shear fractures/faults. Letters denote localities where conjugate fractures are described in Figure 17.

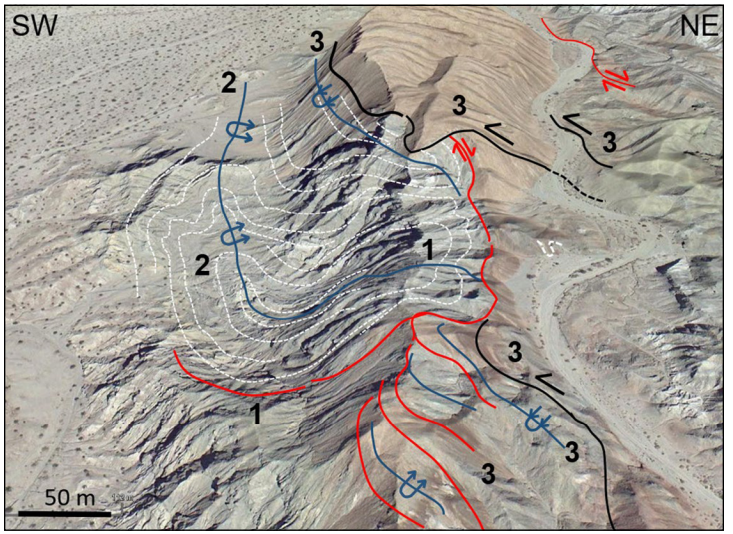

Figure 11. Google Earth digital elevation model (DEM) image of San Andreas fault gouge (light-brown color) adjacent to subdomains A1 and B2 on either side of San Andreas fault (see location in Fig. 4A), viewed northwestward along strike of San Andreas fault. Image demonstrates polyphase kinematic evolution of (1) an initially steep San Andreas fault and splaying upright en échelon folds, (2) reorientation of en échelon folds into parallelism with San Andreas fault ~100 m from San Andreas fault, and (3) truncation by out-of-sequence thrust faults and related folds completely parallel to San Andreas fault, overriding San Andreas fault.

bent into hinge zones of the large, steeply plunging folds of subdomains A1 and A2, thus confirming that the latter folds postdate the subhorizontal en échelon folds. A second generation of steep, axial-planar faults truncate and displace beds right laterally and display dextral, strike-slip fault-surface striations (see below).

Along strike southeastward from subdomain A3 in the Basin block toward Box Canyon, the San Andreas fault gouge zone becomes straighter and narrows to less than 50 m (Fig. 4A); here, en échelon folds are absent. Instead, beds of surrounding Palm Spring and Ocotillo strata are uniform in attitude, strike parallel to the San Andreas fault, dip steeply SW, and are cut by minor, steeply dipping faults subparallel to the San Andreas fault, with strike separation.

Similarly, where the San Andreas fault reappears northwest of Painted Canyon, it has a straight trace over a distance of ~3 km along strike to Red Canyon (Fig. 3). There the San Andreas fault has a 10-m-wide fault core zone subparallel to steeply (70°–80°) SW-dipping upper Palm Spring strata. About 100 m southwest of the San Andreas fault contact, in the Basin block near the contact with the Ocotillo Formation, remnants of tight to isoclinal, San Andreas fault–parallel hinges of steeply plunging folds with steep axial surfaces are preserved within the steeply dipping San Andreas fault–parallel beds, suggesting that the steep fault(s) there formed synchronously with the steeply plunging folds in subdomains A1 and A2.

Folds and Thrust Faults Parallel to the San Andreas Fault

A third set of large-scale deformation features in Mecca Hills is displayed by fold and thrust faults trending NW-SE fully parallel to the San Andreas fault. Field relations show they are superposed upon all previously described structures, locally causing significant modification and even reorientation of both upright en échelon folds and steeply plunging folds and faults (Fig. 4B, cross-sections a-a′, b-b′, and c-c′; Figs. 11 and 12). The San Andreas fault–parallel folds are strongly asymmetric, verging SW, with subhorizontal axes, and gentle, NE-dipping (10°–45°) axial surfaces associated with thrust faults. It is not always easy to distinguish them from the earlier formed en échelon folds, but where they interact, they have different orientations and much wider, thrust-repeated San Andreas fault gouge zones (Fig. 4B). The best example is at the mouth of Painted Canyon (Figs. 3 and 4A), where the Skeleton Canyon fault dies out and the San Andreas fault and other en échelon folds are partly beheaded by steep reverse faults for a distance of ~4 km, defining a thrust lobe (Fig. 3). The reverse character of the faults there is verified by fold data (Fig. 6) and minor reverse shear fractures (see later herein).

In subdomains B1 and B2 (Fig. 4A), a gentle NE-dipping thrust fault emplaces slivers of San Andreas fault gouge on top of and decapitates an en échelon synclinal fold in its footwall (Figs. 4B, cross-section a-a′; Figs. 11 and 12), thus establishing its younger relative age. This thrust also truncates a folded, steep San Andreas fault gouge contact (Figs. 10A and 11), and both limbs of a tight, upright syncline within the San Andreas fault gouge zone itself (Fig. 12). The same thrust links with the Skeleton Canyon fault (Fig. 4B, cross-section a-a′), which, in subdomain B2, also strikes parallel to the San Andreas fault and truncates both limbs of tight en échelon folds there in its footwall (Figs. 7A–7C). A similar fold-and-thrust system exists closer to the San Andreas fault, ~1 km farther southeast in subdomain B2 (Fig. 4B, cross-section b-b′). There, repeated thrust slices of San Andreas fault gouge (red-brown color) comprise remnants of modified en échelon fold hinges and dismembered Palm Spring sandstone beds. The overprinting nature of the San Andreas fault–parallel thrusts is supported not only by the decapitation of en échelon folds, but also by a change in orientation of en échelon folds and faults, from WNW-ESE to NW-SE trends (Fig. 6; subdomains B2 and B3).

The Skeleton Canyon fault in subdomains B4 and B5 also truncates, decapitates, and reorients en échelon folds in the footwall (Figs. 4 and 6). In the hanging wall (Fig. 13), tight, overturned, near-recumbent anticline-syncline folds trend NW-SE subparallel to the San Andreas fault (Fig. 4B, cross-section d-d′). These asymmetric, SW-verging folds probably formed above a ramp below the Skeleton Canyon syncline that makes up the interior of the Central block (Fig. 3; Sylvester and Smith, 1976, 1987). Similar folds are common throughout the Central block, such as in Painted Canyon, where they verge both SW and NE and are accompanied by decapitating reverse/thrust faults (Figs. 14A and 14B).

A major NE-verging, slightly overturned anticline trends NW-SE parallel to the San Andreas fault in Palm Spring strata of subdomain A3 in the Basin block (Figs. 4A and 4B, cross-section c-c′; Fig. 6). Its NE vergence toward the San Andreas fault (Fig. 14C) is opposite to most en échelon and San Andreas

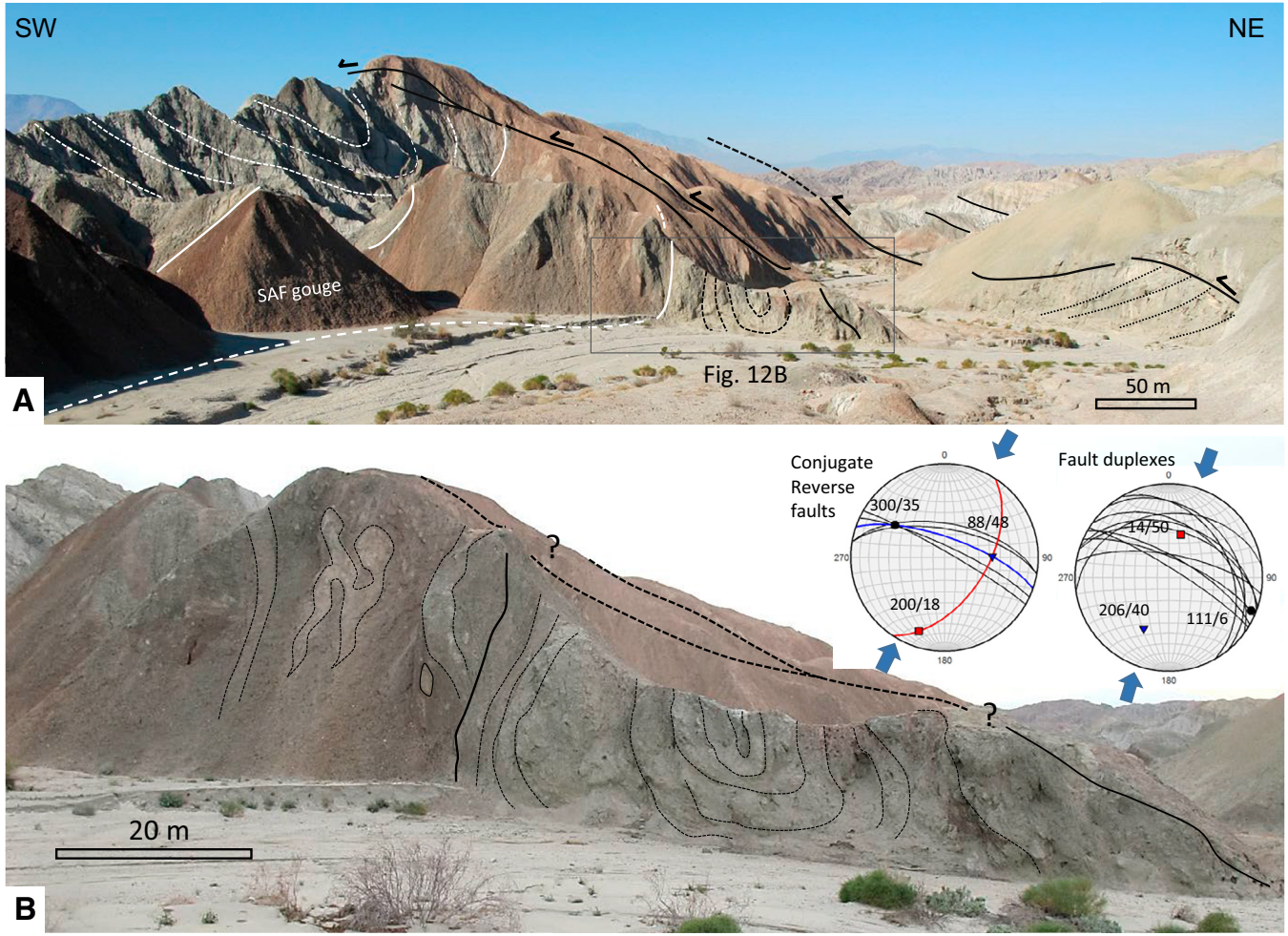

Figure 12. Outcrops with complex fold-and-thrust fault structures adjacent to San Andreas fault (SAF) in subdomain B2, close to subdomain A1 (for location see Fig. 4A). (A) Asymmetric south-verging, synclinal en échelon fold that folds steep contact and red-brown–stained fault gouge (brown color) of San Andreas fault in Basin block. This synclinal fold system is itself truncated by a gently NE dipping (out-of-sequence) thrust fault that cuts both limbs of the fold and refolds the syncline farther SW (see Fig. 11). Tight to isoclinal, upright, synclinal fold in Palm Spring strata is visible northeast of gouge zone in A; this fold is fully decapitated by the out-of-sequence thrust (see Fig. 4B, cross-section a-a'). Thrust is also emplaced upon steeply plunging folds in subdomain A1 (see Fig. 9A). (B) Detailed view of upright isoclinal fold in Palm Spring strata shown in A, which is decapitated by out-of-sequence thrust. Lower-hemisphere stereograms depict shortening strain fields (arrows) from minor conjugate reverse fractures (black great circles), fracture intersections, and duplexes adjacent to the thrust. Strain axes (*z*—red square, *y*—dot, *x*—triangle).

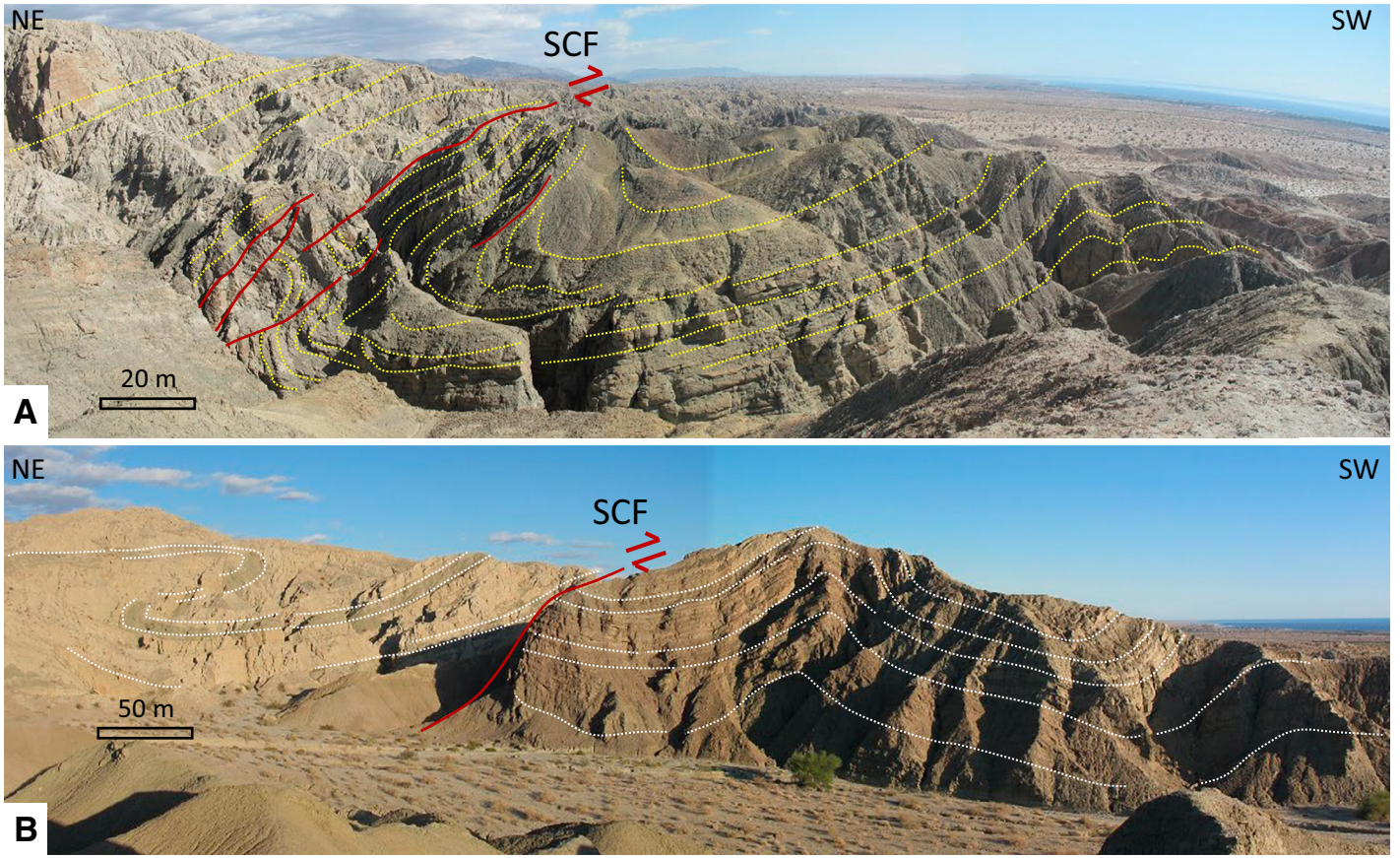

Figure 13. (A) Tight, asymmetric, and SW-verging en échelon fold system in footwall of Skeleton Canyon fault (SCF) in subdomain B4 (same as in Fig. 7D) (for location, see Fig. 4A). Fold is modified, appressed, and reoriented completely parallel to Skeleton Canyon fault (and San Andreas fault) near fault surface; ~200 m farther southwest, same fold is oblique relative to the San Andreas fault. (B) Panorama view of the Skeleton Canyon ramp-generated fault and adjacent structures in subdomain B5. Note several open, upright en échelon folds in upper Palm Spring mudstone strata (right in photo) that are overthrust by younger, upper member Palm Spring arkosic strata (left in photo). Tight recumbent folds are in hanging-wall strata of Skeleton Canyon fault on SW limb of Skeleton Canyon syncline (Sylvester and Smith, 1976, 1987).

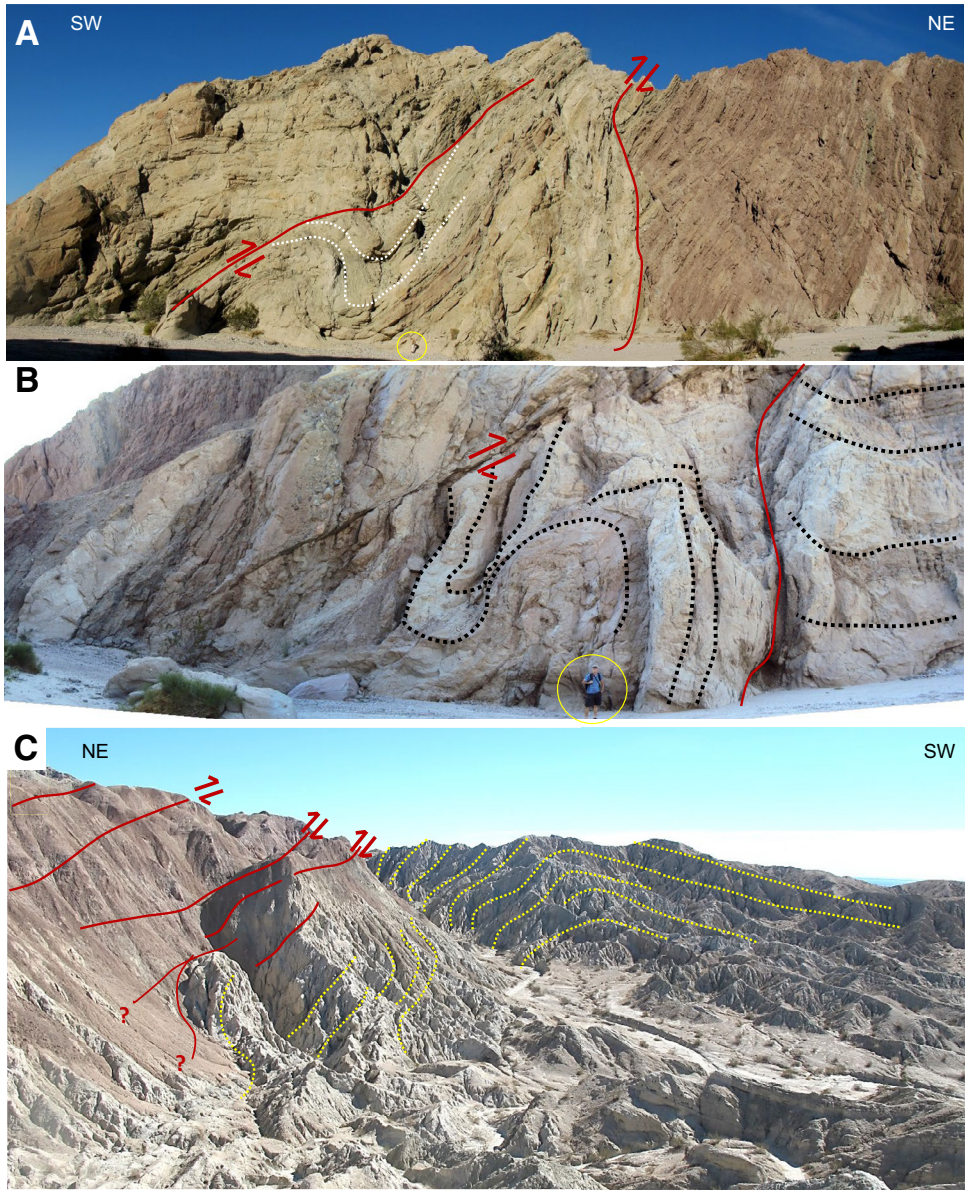

Figure 14. (A) Fold-thrust structures in Central block in Painted Canyon (see Fig. 3). Asymmetric NE-verging fold and related steep reverse fault emplace Palm Spring strata (light-yellow color) against older Mecca conglomerate units (brown color) in the footwall, indicating out-of-sequence thrusting. A small-scale, out-of-sequence thrust fault decapitates both limbs of an earlier fold. Geologist in yellow circle. (B) Planar out-of-sequence thrust decapitates folded and faulted Palm Spring strata in Platform block adjacent to Painted Canyon fault at head of Painted Canyon (see Fig. 3). Geologist in yellow circle. (C) Landscape view of NE-verging anticlinal fold in upper Palm Spring strata of subdomain A3 in Basin block, adjacent to San Andreas fault gouge (red-brown zone, left in photo). Fold trends parallel with San Andreas fault but verges opposite relative to all other fold-thrust faults in the area. A network of smaller-scale, SW-directed imbricate thrust faults and slices of San Andreas fault gouge zone truncates and modifies the fold.

fault–parallel folds in the mapped area. The overturned NE forelimb strata are cut by several SW-directed imbricate thrust slices of San Andreas fault gouge (Fig. 14C). On the opposite back-limb part of the macrofold, the beds dip moderately (40°–60°) SW and are truncated by the Ocotillo Formation, which is now tilted to a dip of ~20°–25° SW (Fig. 3; Fig. 4B, cross-section c-c′, left part). We interpret this contact as a depositional unconformity, limiting the age of San Andreas fault–parallel folding to pre–0.7 Ma (cf. McNabb et al., 2017).

In the area between Red Canyon and Thermal Canyon (Figs. 3 and 15), the San Andreas fault gouge zone changes to a heterogeneous San Andreas fault–parallel unit up to 500 m wide with complex internal structures that are exclusively contractile. Southeast of the mouth of Red Canyon, the steep San Andreas fault gouge zone, associated steep contacts, and Palm Spring strata are folded into a NW-SE–trending, open, upright en échelon anticline (Figs. 15A, 15B, and 16A). Along the interpreted cross section ~250 m farther north (Fig. 15C), a similar but much tighter recumbent fold system is present with San Andreas fault gouge in the hinge zone (Figs. 16B and 16C). Both limbs of this fold are cut by low-angle, NE-dipping and SW-directed thrusts (Figs. 15A–15C), and subhorizontal imbricate slivers of San Andreas fault gouge are emplaced upon the en échelon folded units (Fig. 16B), thus repeating, thickening, and widening the gouge zone. The imbricate gouge slices contain remnants of dismembered Palm Spring strata (Fig. 16B), all suggestive of considerable reorganization and modification of the strata by the overriding San Andreas fault–parallel fold-and-thrust system.

MINOR CONJUGATE SHEAR FRACTURES

Minor sets of conjugate shear fractures abound in the Mecca Hills (Fig. 17) and are considered valid indicators from which to infer the nature of strain based on their specific bisecting orientations and sense-of-shear character relative to folded and faulted bedding (Reches, 1978; Hancock, 1985). Where related to en échelon folds and fold-and-thrust systems, one set of gently dipping (≤30°) conjugate shear fractures intersects parallel with the fold axis (*b* axis), whereas another, steeply dipping (≥60°) fracture set intersects the *a* axis of folds, defining hk0 fractures (cf. Hancock, 1985); therefore, they formed synchronously with major folds and faults (Stearns, 1968; Dunne and Hancock, 1994). Conjugate fractures are present within the San Andreas fault core gouge itself, within en échelon folds and faults, and in domains of superposed, steeply plunging folds and San Andreas fault–parallel fold-thrusts (Fig. 18A). They were used to determine crosscut relations and analyze effects of changing strain fields.

Conjugate shear fracture sets in subdomains B2–B5 of the Central block are in the limbs and hinges of large-scale en échelon folds (Fig. 18A). Most observed fractures strike approximately W-E, parallel to en échelon fold axes (*b* axis), dip moderately northward and southward, and display dominantly reverse bed offsets (Fig. 18A, green great circles). Where present, slickenside striations indicate oblique-reverse, top-to-the-N and top-to-the-S senses of shear (Figs. 18B and 18C) and approximately subhorizontal N-S to NNW-SSE shortening axes (*a* axis), similar to strain estimates for en échelon folds and faults in the Central block (Fig. 6A). Correspondingly steep, conjugate lateral-slip hk0 fractures (Hancock, 1985) in subdomains B2–B5 (Fig. 18A, red and blue great circles) also reveal N-S shortening axes.

Conjugate strike-slip shear fractures in steeply plunging folds in subdomain A1 of the Basin block are widespread in hinge and limb areas (Figs. 10B and 17). They truncate folded sandstone beds at a high angle to bedding in isoclinal fold hinges, but they are parallel to thinned limbs of the same folds (Fig. 10B). Fractures with right-lateral offset strike N-S on average, whereas left-lateral fractures strike NW-SE, yielding a NW-SE–trending shortening axis (Fig. 18A, subdomain A1). By contrast, approximately N-S–directed shortening axes were determined from reverse conjugate fractures in subdomains A1 and A2 (Fig. 18). In areas where en échelon folds bend into steeply plunging folds (subdomains A1–A2), steep fold limbs contain internal fracture sets at low angle to bedding, implying these fractures formed earlier and were tilted/folded and then truncated by the steep conjugate fracture sets described above. This conclusion suggests variable and/or changing local strain fields, multistage formation of shear fractures, and reorientation of older fractures due to overprinting deformation.

Conjugate fracture sets in large-scale folds and thrusts that override the San Andreas fault in subdomain B1 are reverse and contain striations yielding top-to-the-SW displacement and NE-SW shortening directions, perpendicular to the San Andreas fault (Figs. 18A and 19). Similar strain fields were obtained from reverse fractures near the major thrust in subdomain B2 (Fig. 12). Other NW-SE–trending folds, such as the concentric anticline in Palm Spring strata of subdomain B1, are truncated by NW-SE–striking extensional fracture sets that converge toward the anticline's hinge zone (Fig. 19A). Small-scale normal faults, asymmetric folds, and related low-angle conjugate reverse fault sets are also present on limbs of the Skeleton Canyon syncline in subdomain B1 (Figs. 18A and 19B) and in hanging-wall strata of the Skeleton Canyon fault in subdomains B2 (Fig. 20) and B5 (Fig. 13), all yielding NE-SW shortening axes perpendicular to the San Andreas fault.

In areas where overprinting fold-and-thrust deformation is interpreted, younger fracture sets consistently truncate and/or modify the older ones. For example, in subdomain B2 near the Skeleton Canyon fault (Fig. 4A), en échelon folded strata are bent by San Andreas fault–parallel fold-and-thrust systems, resulting in steeper, more irregular attitudes (Fig. 20). Conjugate reverse faults in en échelon fold limbs of the footwall to the Skeleton Canyon fault (Figs. 20A and 20B) record NNW-SSE shortening, whereas fractures in the hanging wall record a more variable, NE-SW direction of shortening (Figs. 20C and 20D). Similarly, low-angle and steep conjugate fracture sets exist in subdomains B5 (Central block) and A3 (Basin block), recording both N-S and NE-SW shortening directions (Fig. 18). In the Thermal Canyon area, conjugate reverse fractures are present in the SW-dipping forelimb of complexly folded Palm Spring strata in the footwall of San Andreas fault–parallel thrust slivers (Fig. 15C), and these fractures reveal NE-SW shortening, matching estimates from the large-scale folds (Fig. 15D). Inside the San Andreas fault gouge itself, steep minor faults have subhorizontal striations indicating right-lateral displacement (Fig. 15E).

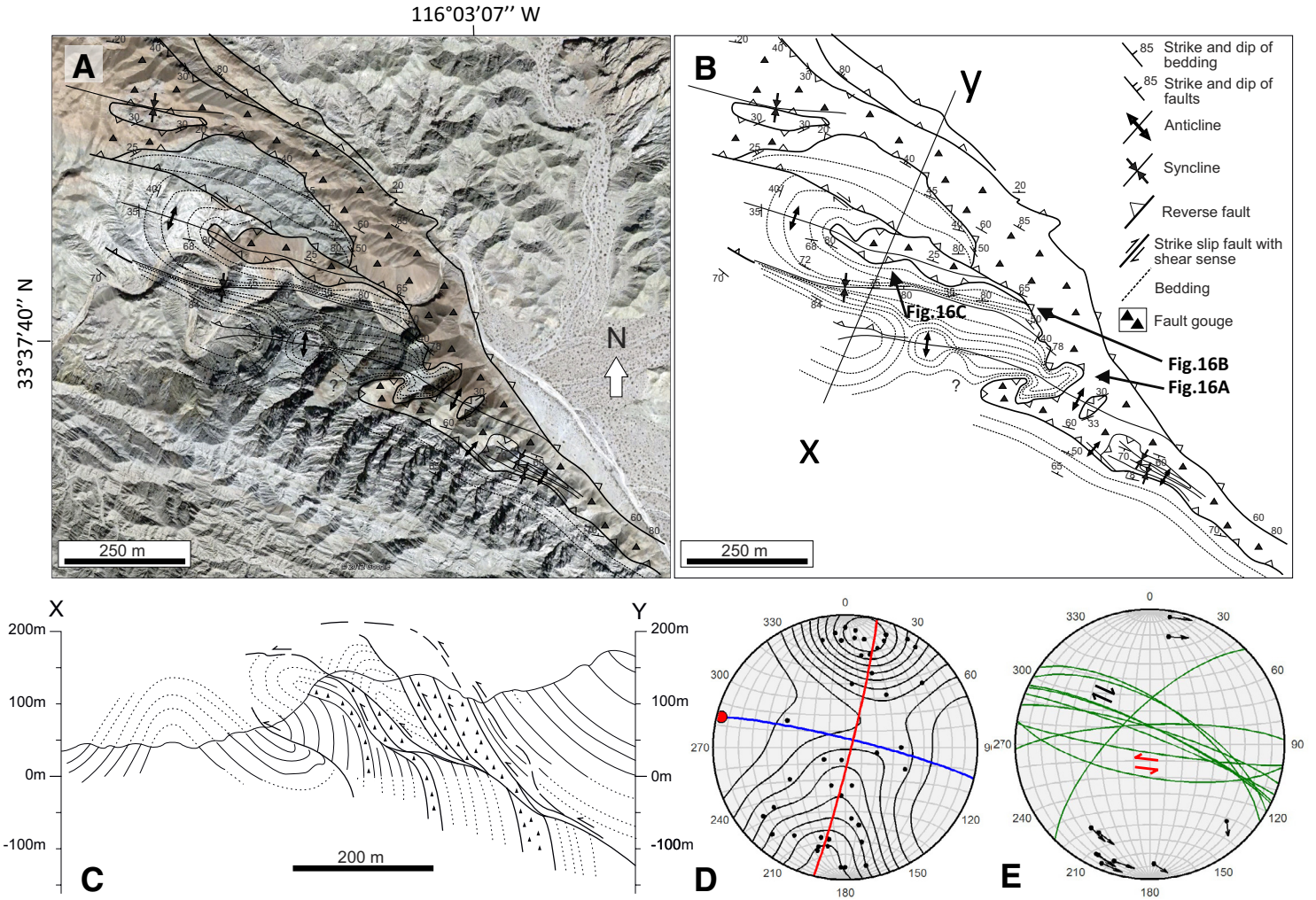

Figure 15. (A) Geologic map of Red Canyon, near Thermal Canyon (see Fig. 3 for location), superposed upon Google Earth digital elevation model image. Wide part of San Andreas fault gouge (red-brown) separates associated fold-and-thrust fault structures. (B) Interpreted structure map of same area as in A. Note folding of gouge contact in south by upright anticline-syncline pairs, and gouge present in hinge zone of large-scale anticline. (C) Interpreted geologic cross-section X-Y, Red Canyon, depicting the complex geometry of fold-and-thrust fault structures. Note presence of open asymmetric en échelon fold in left part of section, and a much tighter recumbent fold in footwall of thrust sheets in middle part of section. Fold is attenuated, recumbent, and oriented NW-SE parallel to San Andreas fault. Thrust slivers comprise folded remnants of Palm Spring strata and imbricated gouge; some of these slivers are underlain by a near-horizontal out-of-sequence thrust that decapitates the en échelon folds. (D) Lower-hemisphere stereogram of contoured poles to bedding (left diagram) in footwall of main thrust sheet, indicating girdle arrangement (red line) caused by upright folding (axes, red dot) and axial surface (blue girdle) nearly parallel to the San Andreas fault. (E) Small-scale conjugate shear fractures (green circles) with slickensides, plotted as slip-linears, i.e., pole of fault in center of a line with arrow representing movement (M-) plane (Aleksandrowski, 1985).

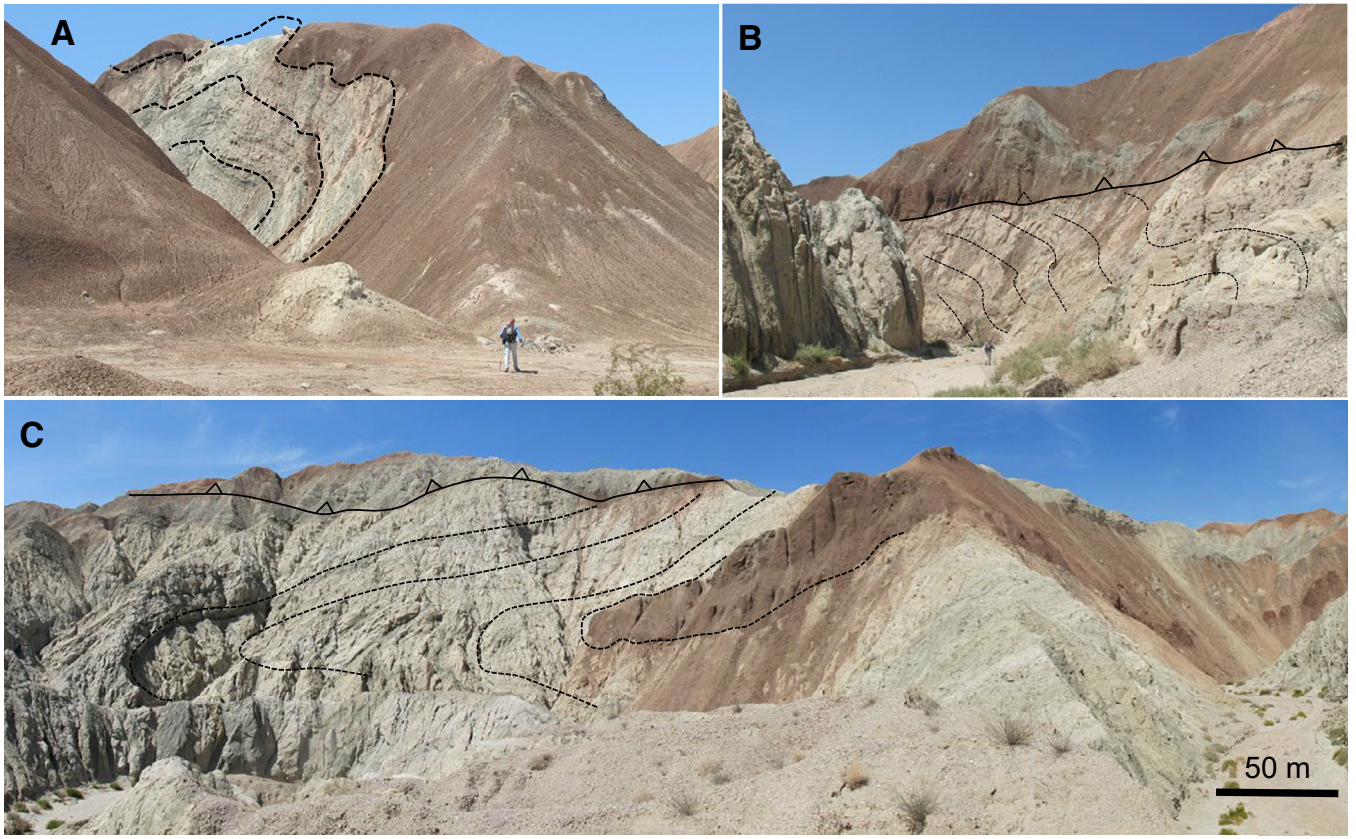

Figure 16. Outcrop photographs of San Andreas fault gouge zone and surrounding Palm Spring strata in Red Canyon (for location, see arrows in Fig. 15B). (A) Steep contact with Palm Spring beds folded by upright, asymmetric en échelon folds. View west. (B) Horizontal thrust contact between San Andreas fault gouge and underlying, folded, and steeply dipping Palm Spring strata (left part of photo) in Red Canyon. Slivers of Palm Spring beds are preserved inside breccia. View west. (C) Tight, recumbent fold in Palm Spring beds with San Andreas fault gouge in its hinge zone. Fold is cut by a thrust sheet on the ridge consisting of horizontal Palm Spring units and San Andreas fault gouge. View NW.

DISCUSSION

The structural data presented here favor polyphase transpression for the wedge/flower-like structure of San Andreas fault in the Mecca Hills (Fig. 3), rather than synchronous transpression (Sylvester, 1988), although the ages of the three deformation stages are not fully dated. The only absolute timing constraints on the kinematic events are from the Bishop Tuff in the uppermost Palm Spring Formation (0.765 Ma) and tilted Ocotillo Formation (<0.7 Ma) strata postdating the tuff, yielding timing for the fold-and-thrust structures (third kinematic event) close to the unconformity below the Ocotillo Formation on eroded San Andreas fault–parallel folds (Fig. 4B, cross-section c-c′). Furthermore, the consistent tilting of Ocotillo deposits subparallel to the San Andreas fault, and the lack of observed dextral offset across the study area between the Ocotillo deposits and a different source terrane suggest that the late kinematic event postdates 0.7 Ma and may be still ongoing.

We postulate that events in Mecca Hills started with distributed simple shear (cf. Tikoff and Teyssier, 1994), followed by partly partitioned deformation (cf. Leever et al., 2011a), and ended with full (?) strain partitioning, which in the Mecca Hills was dominantly pure shear shortening strain (cf. Mount and Suppe, 1987; Miller, 1998). Below, we argue for this succession of events, first by summarizing key relative timing and overprinting relationships, second by discussing fault architecture, kinematics, and changing strain fields (Fig. 21), third

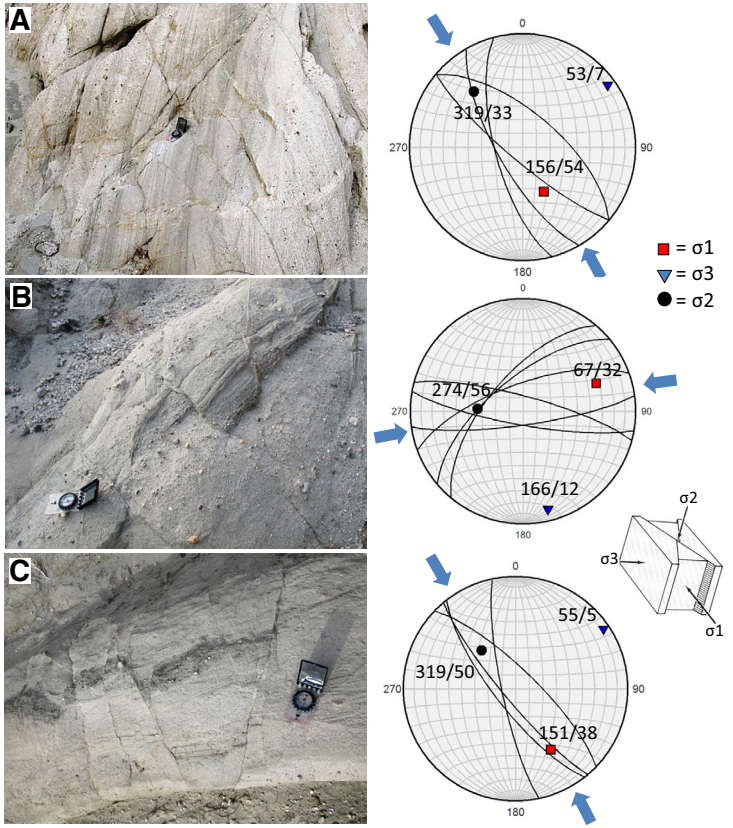

Figure 17. Outcrop-scale examples of steep, conjugate strike-slip fracture sets from various small-scale folds in hinge zone of steeply plunging fold in subdomain A1 of Basin block. Localities a, b, and c are shown in Figure 10B. Fractures cut steep Palm Spring sandstone beds near hinge and/or on limbs of subvertical folds. Lower-hemisphere stereograms show conjugate fractures as great circles, where blue arrows indicate axis of shortening strain, and calculated stresses (σ1, σ2, σ3) are shown as colored symbols.

by considering possible mechanisms of formation of structures in the transpressional wedge (Fig. 22), and finally by considering possible regional implications.

Summary of Relative Timing and Overprinting Relations

The main arguments for a polyphase, three-stage kinematic evolution for structures in the Mecca Hills are: (1) the consistent bending and reshaping of the presumed, initially straight, proto–San Andreas fault trace (Figs. 4A and 6B), (2) the bending of the obliquely oriented first-stage en échelon folds, including the Skeleton Canyon and related faults, from highly oblique into almost complete parallelism with the San Andreas fault trace (Figs. 4A and 6B), and (3) a consistent late kinematic overprint of SW-verging fold-and-thrust belt structures (Figs. 12–14). In addition, a change in attitude and/or refolding of horizontal-upright en échelon folds oblique to the San Andreas fault into steeply plunging tight/isoclinal folds parallel to the San Andreas fault (Figs. 10 and 11) is used as evidence for progressive and/or episodic lateral shearing during the second kinematic stage. Finally, small-scale conjugate strike-slip and reverse shear fractures exist in all structural associations, displaying overprinting relations and changing attitudes that are largely in support of the polyphase history (see discussion below).

Fault Architectures and Kinematic Evolution

Stratigraphic, paleoseismic, magnetic, and gravity studies imply that the San Andreas fault entered the Salton Trough as a major, dextral strike-slip fault ~6 m.y. ago and occupied a steep, preexisting Basin and Range normal fault (Frost and Martin, 1982; Herzig et al., 1988; Stock and Hodges, 1989; Winker and Kidwell, 1996; Atwater and Stock, 1998; Dorsey et al., 2011). That deformation created a steep and narrow fault gouge zone, which transects Pliocene Palm Spring Formation strata. Such relations are preserved only between Red and Painted Canyons (Fig. 3) and in subdomains A3 and B5, where fault gouge contacts are steep and emerge upward into hinges of upright, en échelon folded Palm Spring strata (Fig. 4B, cross-section d-d′). Elsewhere along the San Andreas fault strand in Mecca Hills, most of these steep, early faults and fault gouge contacts were folded, overprinted, cutoff, reactivated, or concealed by younger folds and faults, and so relics of the initial deformation phase are difficult to recognize.

First Stage—Distributed Simple Shear

The first main step in the evolution of structures along San Andreas fault was formation of open, concentric, en échelon folds and steep reverse and lateral faults, as exemplified by the Skeleton Canyon fault where it branches out from the steep San Andreas fault in subdomains B1 and B2 (Fig. 21A). The branching may have produced a restraining bend on the north side of the San Andreas fault, where slip was transferred into a left-bending zone that connected en échelon fold-fault structures (cf. Woodcock and Fischer, 1996; Wakabayashi et al., 2004). The Skeleton Canyon fault then initiated as a right-bend, dominantly oblique-slip, en échelon fault (R-shear) during distributed deformation.

Upright en échelon folds and steep subsidiary splay faults commonly form at an angle of 30°–45° to a steep, strike-slip boundary fault (San Andreas fault) in uniformly distributed, simple shear deformation (cf. Mount and Suppe, 1987; Sylvester, 1988; Jamison, 1991; Miller, 1998; Titus et al., 2007). However, most observed en échelon folds in Central block domains (B2–B5) initiated at a high angle to San Andreas fault and then changed to sigmoidal traces and show

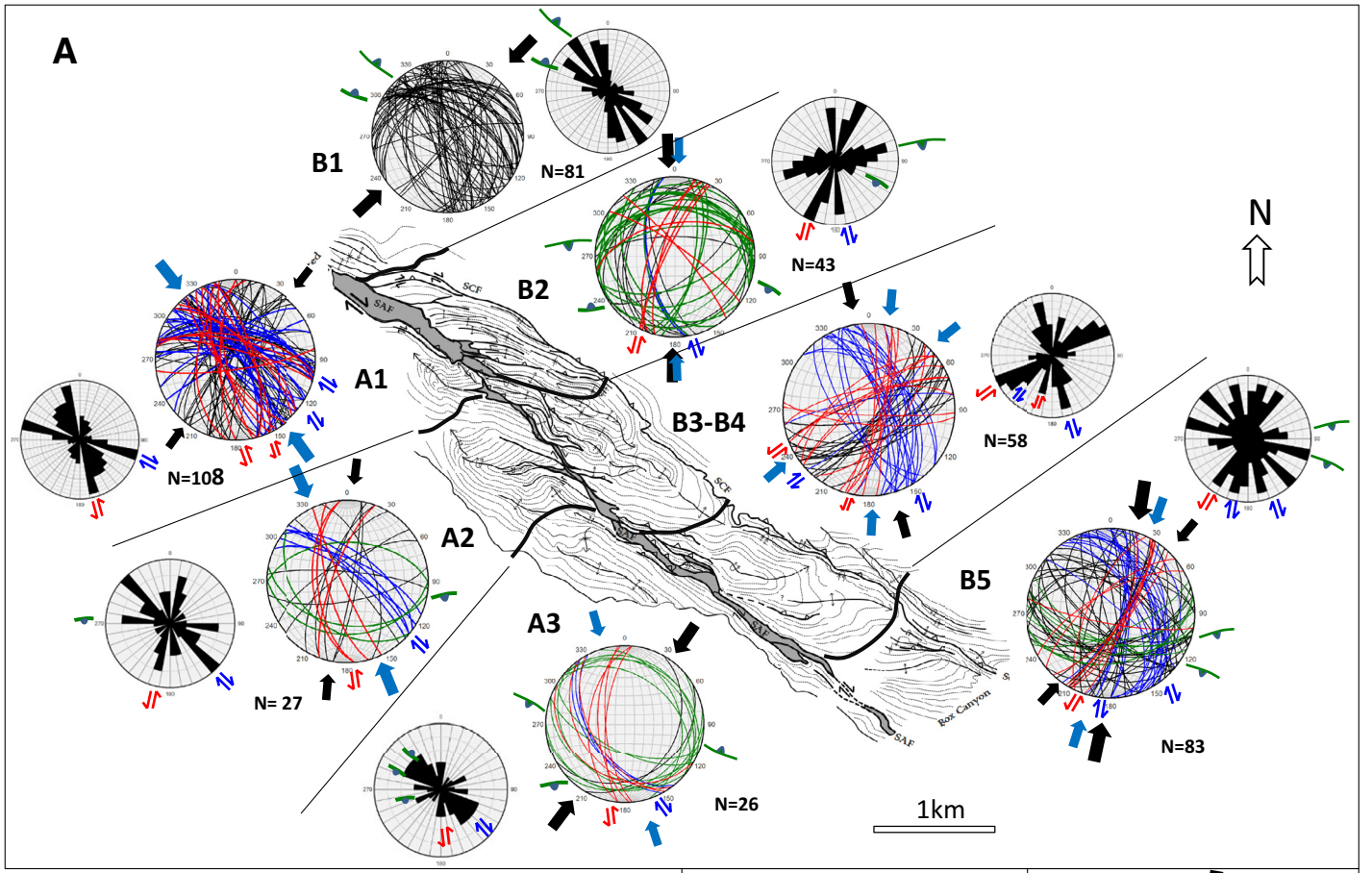

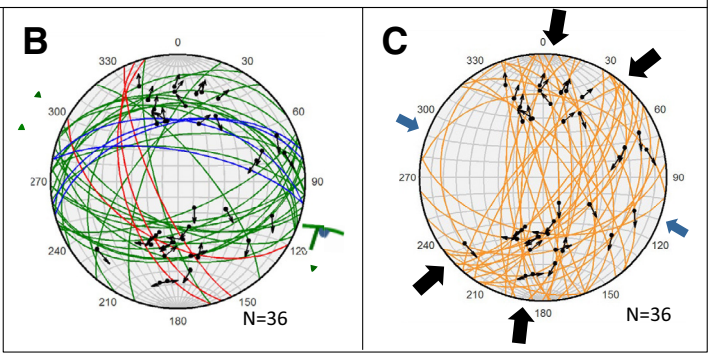

Figure 18. (A) Structural orientation and kinematic data for minor shear fractures in study area, presented in lower-hemisphere, equal-area stereograms and rose plots. Each stereogram contains fracture data in Palm Spring strata collected in the designated subdomains A1 to A3 in Basin block and B1 to B5 in Central block. Subdomains on map are same as in Figure 4. Individual fractures in stereograms are plotted as great circles, where: green—reverse/thrust fractures, blue—right-lateral fractures, red—left-lateral fractures, black—undifferentiated (all types, including extensional). Lateral shear senses are shown by blue half arrows. Reverse/thrust faults are shown as green lines with triangle pointing in the direction of hanging wall. *N*—number of measured fractures. Local shortening directions (*x* axis) were determined from average conjugate strike-slip faults (blue filled arrows) and reverse faults (black filled arrows). Arrow size indicates relative number of shortening axes determined. Rose plots indicate main and subsidiary fracture trends, with kinematics of each trend added from the stereograms, when possible. (B) Equal-area, lower-hemisphere stereograms of all small-scale faults that contain slickensides (green—reverse, blue—dextral strike-slip, red great circles—sinistral strike-slip) from the study area indicated as slip-linear plots (Aleksandrowski, 1985), i.e., pole of fault in center of a line with arrow representing the movement (M-) plane. (C) Plot of M-planes from B (yellow-colored great circles), defined as planar surface through pole of fault and intersection of lineation with fault surface (Aleksandrowski, 1985). Note estimated shortening directions (arrows) from presence of several kinematic groups; top-to-the-S (reverse), top-to-the SW (oblique-sinistral reverse), top-to-the N (reverse), top-to-the NE (oblique-dextral reverse), and sinistral strike-slip, respectively. Abbreviations: SAF—San Andreas fault, SCF—Skeleton Canyon fault.

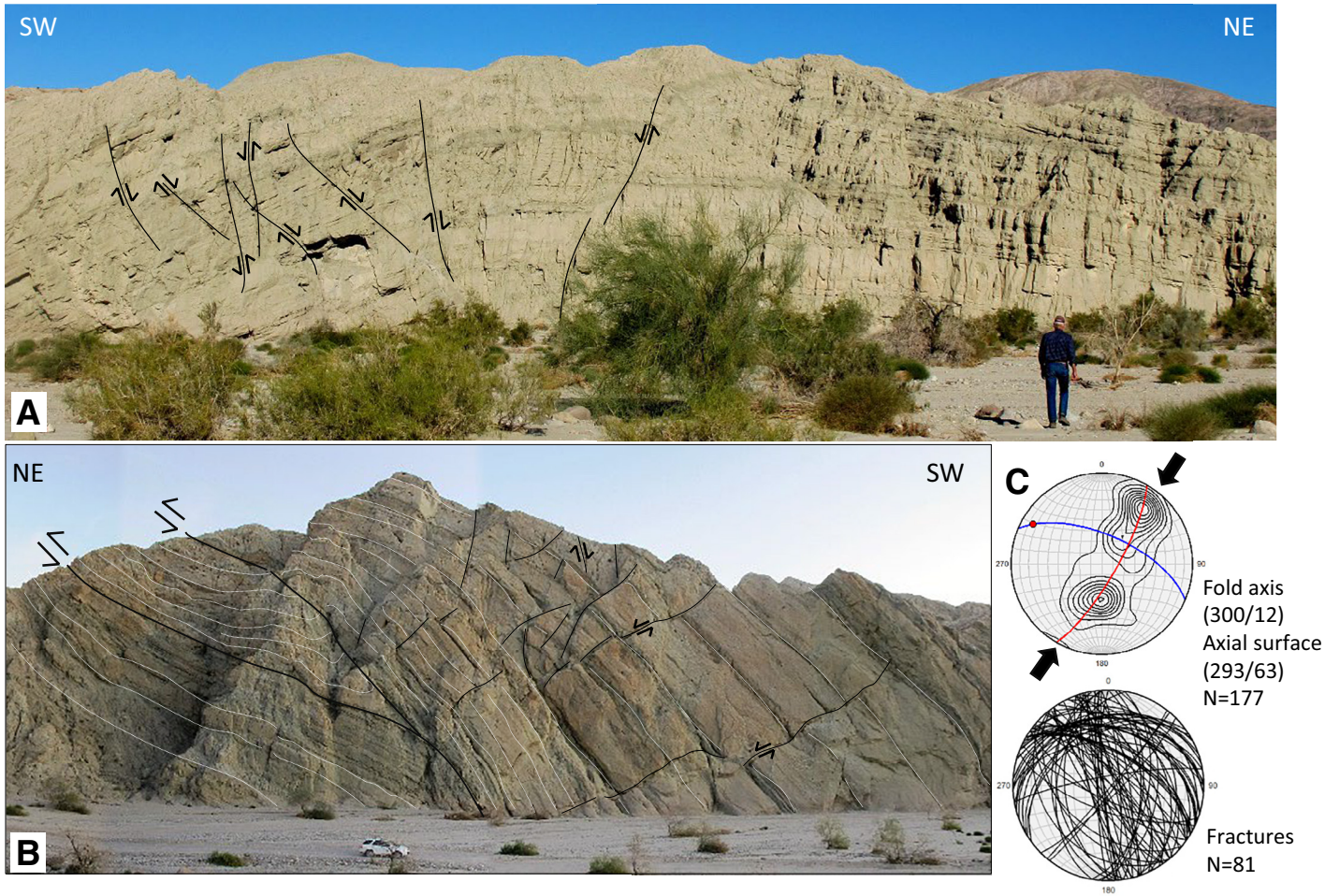

Figure 19. (A) Upright anticline in lower Palm Spring strata on northwest side of Painted Canyon, Central block, containing numerous, steep, NW-SE–striking extension fractures (interpreted black lines) that converge toward hinge. (B) SW-dipping strata in NE limb of Skeleton Canyon syncline in Painted Canyon, with a NE-verging fault-propagation fold and related, out-of-sequence thrust on the northeastern flank of Skeleton Canyon syncline (red lines), in addition to fold-thrust–related extensional fractures (black lines) in back-limb strata of fold. (C) Lower-hemisphere stereograms of folded upper Palm Spring beds (contoured poles, above) and shear fractures (black great circles, below), undifferentiated, in Central block adjacent to Painted Canyon. Contoured poles define two point maxima representing limbs of San Andreas fault–parallel anticline-syncline systems (see Fig. 3), whereas small-scale reverse and extension fractures are consistent with a NE-SW shortening direction perpendicular to the San Andreas fault.

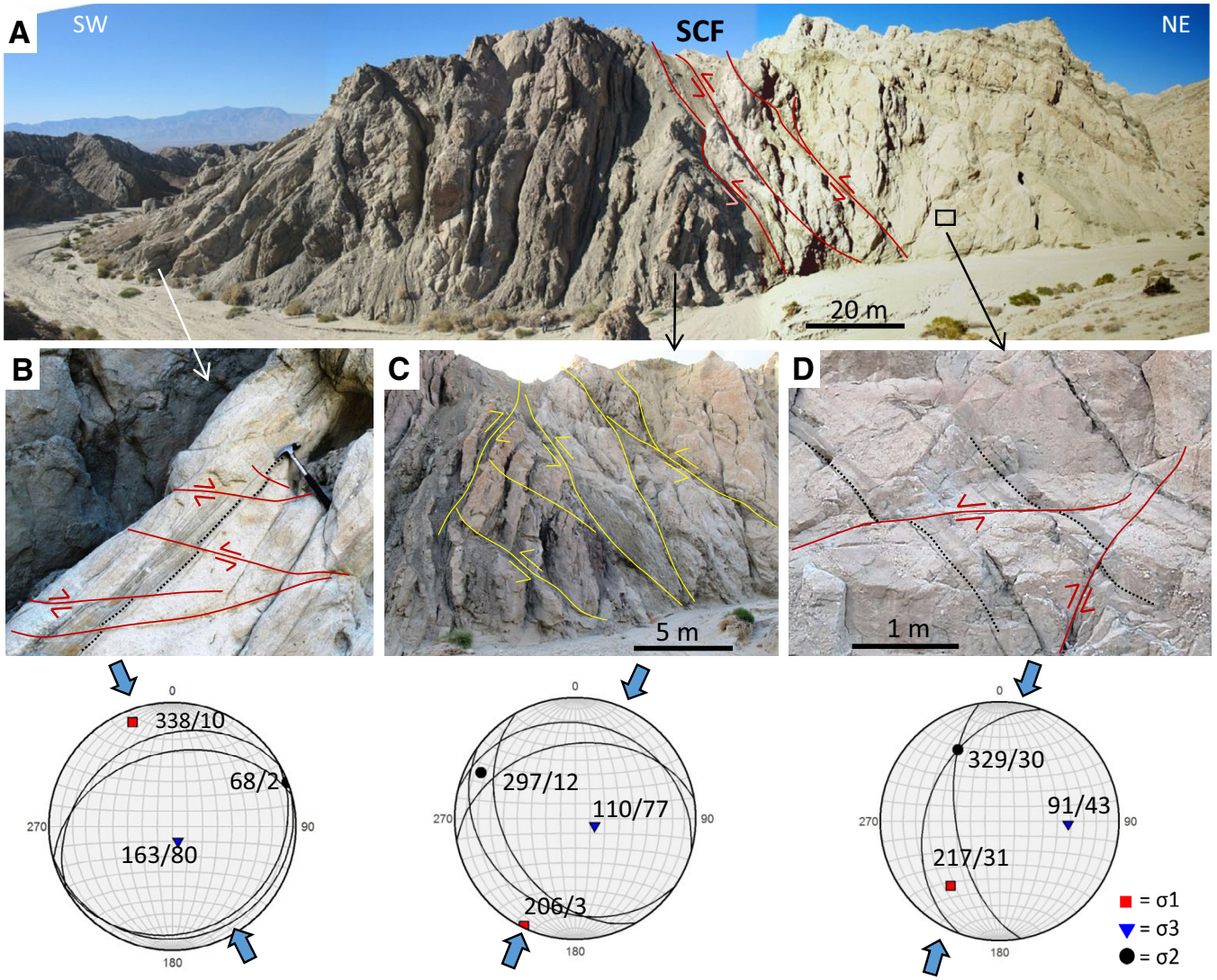

Figure 20. (A) Skeleton Canyon fault (SCF) exposed in subdomain B2 (for location, see Fig. 4A). Folds in upper Palm Spring mudstone (left in photo) are overthrust by younger, upper member Palm Spring arkosic strata of the Central block (right in photo). Thrust reoriented and decapitated en échelon folds in its footwall (compare with Figs. 7A–7C), indicating out-of-sequence thrusting. Folded footwall strata contain minor shear fractures formed in succession due to changing strain fields. (B) Conjugate reverse fracture set in en échelon folded footwall strata, and lower-hemisphere stereograms of representative small-scale, reverse conjugate faults (great circles), with calculated shortening axes (blue arrow) and paleostresses. (C–D) Conjugate reverse fractures from thrust zone and hanging wall of Skeleton Canyon fault, and corresponding stereograms, indicating late-stage, San Andreas fault–perpendicular shortening. See text for further explanation.

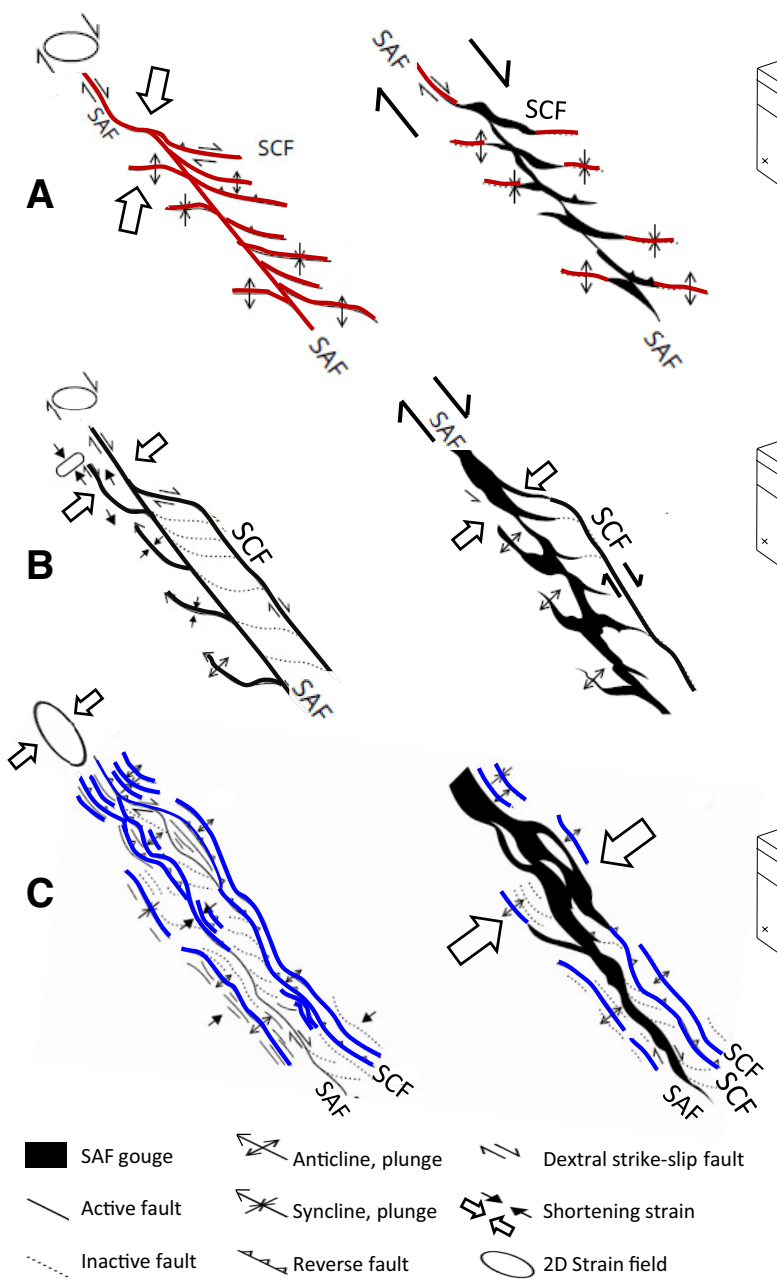

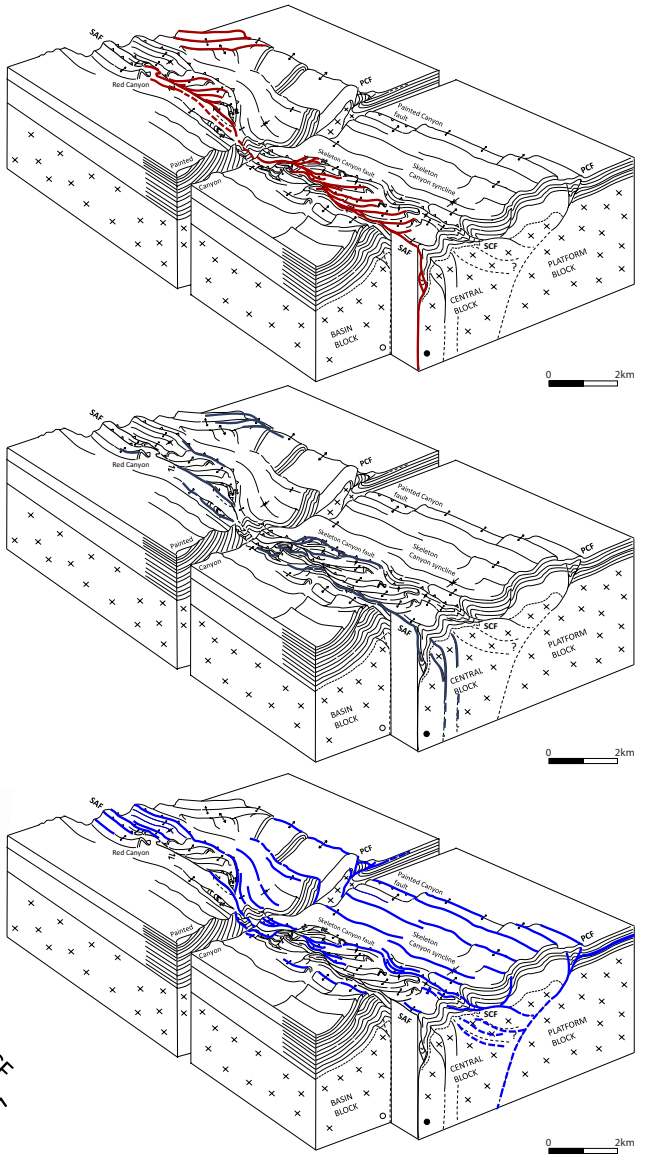

Figure 21. (A–C) Three-stage kinematic evolution of structures in Mecca Hills segment of San Andreas fault southeast of Painted Canyon (see Fig. 4A) outlined in map view as fault and fold relations (left) and San Andreas fault gouge zone architecture (center, black areas). Block diagrams (right) show the part of the flower structure that was active at that point in the evolution of the structure, corresponding with the San Andreas fault and related faults in Mecca Hills. Abbreviations: SAF—San Andreas fault, SCF—Skeleton Canyon fault; PCF—Painted Canyon fault. Color code: red faults—first stage; thick black faults—second stage; blue faults—thrid stage. (A) First kinematic stage with distributed simple shear strain along an initially steep, linear, and narrow part of San Andreas fault generates oblique en échelon folds and reverse faults about 40°–45° to San Andreas fault trace. San Andreas fault gouge migrates outward into the fold hinges. Note initiation of Skeleton Canyon fault in left-bend stepover zone linked with en échelon faults. (B) Second kinematic stage with oblique (partly) strain partitioning, due to renewed, localized strike-slip shearing along the San Andreas fault and Skeleton Canyon fault. Oblique strain partitioning caused reorientation of en échelon folds into steeply plunging folds, by local tectonic wedging, and rearranging of en échelon faults (e.g., Skeleton Canyon fault) parallel to San Andreas fault. (C) Third stage of full strain partitioning, producing San Andreas fault–parallel fold and thrust structures emplaced upon and partly reactivating previously formed structures, in a San Andreas fault–perpendicular shortening strain field. Note also how rotation of en échelon fold hinges into parallelism with San Andreas fault changes linearity of San Andreas fault.

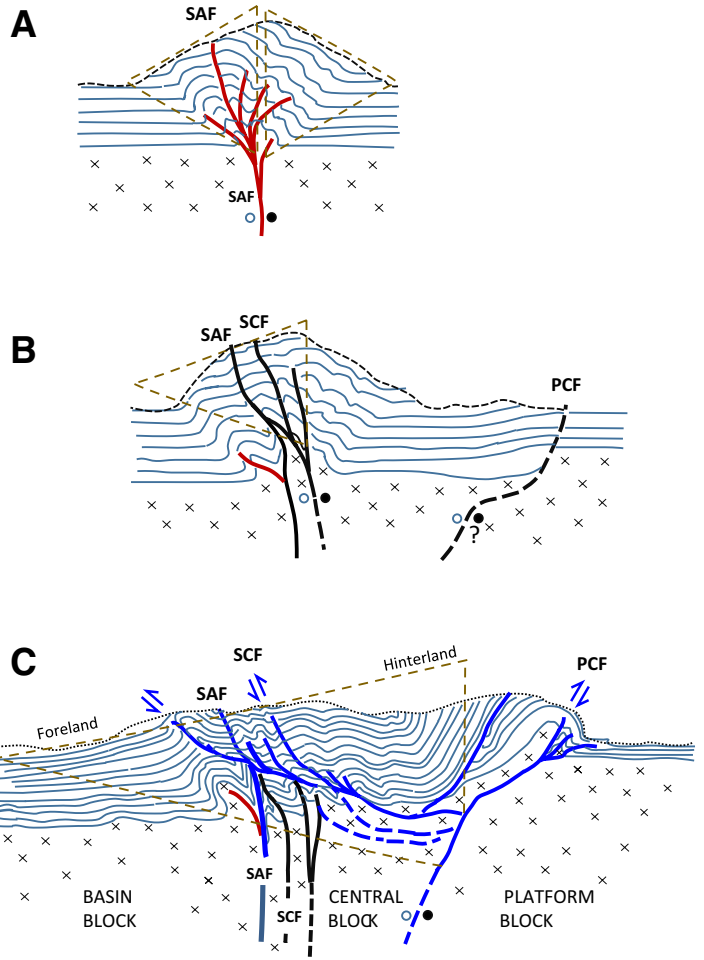

Figure 22. Interpretative, conceptual kinematic evolution of the Mecca Hills transpressional flower-structure (wedge) geometry as outlined in cross-section view of the area between Painted Canyon and Box Canyon (Fig. 4A); not to scale. (A) First stage—formation of symmetric and narrow uplift wedge by strike-slip–dominated transpression and distributed simple shear strain along master San Andreas fault (SAF). Wedge geometry is oversteepened (supercritical) and thus unstable. (B) Change to partly partitioned deformation, which slightly broadens and lowers the wedge. Strike-slip component is localized to Skeleton Canyon fault (SCF), and possibly also the Painted Canyon fault (PCF), whereas the shortening component affects areas in the Basin and Central blocks. (C) Growth of an asymmetric, broad composite, fold-thrust wedge prism with SW-directed thrusts that decapitate and mask the early San Andreas fault trace, lowering the taper to critical shape. Note these thrusts are still linked to the early-stage, steep Skeleton Canyon fault at depth, and this fault is reactivated as a back thrust/ramp below the Skeleton Canyon syncline, relative to the NE-directed, basement-seated Painted Canyon fault at the boundary to the Platform block. The strike-slip component was transferred either to the Painted Canyon fault, or another nearby fault. See text for further explanation.

a lower angle between 30° and 10° to the San Andreas fault (Fig. 4A). In subdomains B4 and B5, we postulate that the en échelon fold hinges extended in length from the San Andreas fault until they merged into the subsidiary Skeleton Canyon fault, where the angle is almost zero degrees to the San Andreas fault (Fig. 4A). These angular changes suggest alternating clockwise and counterclockwise horizontal rotation of en échelon fold hinges by up to 30°, and rotation of the stress triad around the vertical axis (σ_2; Tikoff and Teyssier, 1994; Burbidge and Braun, 1998; Leever et al., 2011a). We favor initial 30°–45° oblique fold hinge migration during a progressive, evolving, distributed simple shear stage, which first localized the simple shear component on several en échelon faults below the folds and then the San Andreas fault became quiescent while strain was transferred along bends and/or stepovers; finally, San Andreas fault slip resumed, causing right-lateral displacement and hinge rotations.

Kinematic data for en échelon folds (Fig. 6A) and minor shear fracture sets in subdomains B2–B5 support distributed simple shear, yielding N-S–directed shortening (Fig. 18), as expected in a strike-slip–dominated folding event (Sylvester, 1988). Strain axes inferred from both reverse and strike-slip conjugate fractures, relative to the en échelon folds, match each other as well (Fig. 18), thus indicating a consistent subhorizontal N-S hinge-perpendicular shortening direction during the en échelon folding event.

Second Stage—Partly Partitioned Simple and Pure Shear

The strain field that reshaped the upright en échelon folds into steeply plunging folds subparallel to the San Andreas fault in subdomains A1 and A2 of the Basin block (Figs. 10 and 11) must have differed from uniform distributed simple shear. We favor a model in which the distributed strike-slip component became partly localized onto nearby or earlier-formed faults such as the proto–San Andreas fault itself and/or the Skeleton Canyon fault (Fig. 21B). If so, then shortening strain in subdomain A1 was probably controlled by proximity to the steep San Andreas fault bend or stepover zone, where, for example, the Skeleton Canyon fault formed (Fig. 21B; cf. Wakabayashi et al., 2004).

During progressive simple shear strain, en échelon fold hinges may rotate in the *x-z* (horizontal) plane of the two-dimensional (2-D) strain ellipse (Sanderson and Marchini, 1984; Bürgmann, 1991; Titus et al., 2007). Additional rotation of fold hinges into a steep plunge, in a three-dimensional (3-D) strain field, may occur if strike-slip strain is localized upon a nearby steep planar fabric (cf. Bergh et al., 2010). Our data suggest that en échelon fold hinges rotated to a steep plunge due to strike-slip displacement, whereas fold shapes were appressed by enhanced contractile strain perpendicular to the San Andreas fault (Figs. 10 and 11). Analog interpretations have been proposed to account for dip-slip, contractile deformation indicators southwest and northeast of the San Andreas fault in central-northern California (Page, 1990; Tavarnelli and Holdsworth, 1999). The triggering mechanism may have been increased slip or shear stress on favorably oriented steep faults (San Andreas fault or Skeleton Canyon fault), or steeply dipping beds in the Basin block.

Similar partitioned deformation and controlling factors for subvertical (3-D) reshaping of fold geometries have been demonstrated in other transpressive settings (Maher and Craddock, 1988; Maher et al., 1995; Teyssier and Tikoff, 1998; Braathen et al., 1999; Garde et al., 2002; Holdsworth et al., 2002; Tavarnelli et al., 2004; Bergh et al., 2010; Leever et al., 2011a, 2011b). Such reshaping is also well supported by analog models (Leever et al., 2011a, 2011b), which show that partly partitioned strain may lead to a narrowing of the fold and fault zone adjacent to the major fault (as in subdomains A1 and A3), whereas widening may indicate ongoing distributed deformation (as in subdomain A2).

Further support for fold hinge rotation is obtained from fold and shear fracture data, where shortening axes change from approximately N-S in subdomain A2 to NE-SW in subdomain A1 (Figs. 6A and 18A). This change is consistent with extension parallel to the fold axis and shortening perpendicular to fold axis, as is required to explain rotational deformation by strike slip in a 2-D simple shear strain field (Bürgmann, 1991; Tikoff and Teyssier, 1994; Burbidge and Braun, 1998; Titus et al., 2007). By contrast, strain data from conjugate strike-slip fractures in subdomain A1 indicate San Andreas fault–parallel shortening (NW-SE; Figs. 10 and 18A). Such shortening may be due to San Andreas fault–parallel reactivation and local tectonic wedging (Fig. 21B), similar to orogen-parallel movements in oblique-convergent settings (Jones et al., 1997; Holdsworth et al., 2002). An alternative is triclinic transpression caused by disharmonic folding and accommodation within the large-scale fold hinge in subdomain A1 (Fig. 10; Jones et al., 2004). A simpler explanation is that San Andreas fault–parallel strike-slip fractures are P-shears formed by resumed right-lateral shearing along a second fault strand of the San Andreas fault (Fig. 21B), thus marking a change from distributed to partitioned strain.

Third Stage—Full Strain Partitioning (?)

San Andreas fault–parallel fold-and-thrust fault structures have geometric characteristics that resemble those of classic contractile fold-and-thrust belt systems (Bally et al., 1966; Price, 1986; Boyer and Elliott, 1982; Butler, 1982; Jamison, 1987, 1991; Erslev, 1991; Molinaro et al., 2005). However, they also have many features in common with structures characterizing transpressional mountain ranges (e.g., Harland, 1971; McCaffrey, 1992; Dallmann et al., 1993; Bergh and Grogan, 2003; Bergh et al., 1997, 2000; Braathen et al., 1999).

The lobate shape of the fold-and-thrust structures at the mouth of Painted Canyon, in the Central block (Fig. 3; Sylvester and Smith, 1976, 1987), can be explained by unequal, SW-directed thrust sheet movement and reactivation of the underlying San Andreas fault and en échelon folds. This lobe was possibly limited laterally by oblique ramp faults. We postulate that to the southeast, oblique thrust-ramp faults may have propagated upward from the Skeleton Canyon fault during the late-stage shortening event (Fig. 21C). If the Skeleton Canyon fault initiated as an oblique, strike-slip fault during the distributed simple shear stage, i.e., right- and left-bend en échelon faults on either side of Painted Canyon (Fig. 3), then these early en échelon faults controlled the successive lobe-shaped evolution and late-stage reactivation of the Skeleton Canyon fault as a thrust.

SW-directed fold-and-thrust structures also exist in subdomains B1 to B5 (Fig. 4). They include fore-thrusts, back-thrusts, ramp-flat thrusts, and related fault propagation folds (Figs. 13 and 19), and they all formed by synchronous, SW- and NE-directed, in-sequence thrusting (cf. Morley, 1988), where new thrusts developed piggyback in the footwalls of previous en échelon folds (Butler, 1987). Fold-related extensional fractures suggest extension, or transtension, of the fold's crest due to bed-parallel flexural slip folding (Fig. 19A). SW-directed out-of-sequence thrusting (cf. Morley, 1988), where new thrusts developed in the hanging walls of previous faults as overstep or break-back thrusts (Butler, 1987), occurred later upon gently NE-dipping thrust faults (Figs. 11, 12, and 14). Multiple fault slivers were emplaced over earlier, en échelon folds and steep faults (San Andreas fault and Skeleton Canyon fault). Similarly, minor conjugate reverse and strike-slip shear fractures also formed by NE-SW–directed, San Andreas fault–perpendicular shortening (Fig. 18), supporting a switch to dominantly partitioned shortening strain (Figs. 21C).

The large-scale San Andreas fault–parallel fold in subdomain A3 verges NE and modifies the steeply plunging fold hinges in subdomain A2 (Fig. 14C), indicating that San Andreas fault–perpendicular shortening in the Basin block postdated the second kinematic stage. This fold is cut by still-younger, but oppositely NE-dipping, thrusts and imbricate slivers from the adjacent Central block (Fig. 14C), supporting a switch to SW-directed (foreland) shortening strain (Figs. 18 and 21C).

The wide fold-and-thrust structures in Red Canyon (Fig. 15) may have formed by repeated imbricate thrusting of San Andreas fault gouge and recumbent isoclinal folding along the San Andreas fault itself. Some thrusts were possibly still linked to the steep San Andreas fault and/or steep en échelon faults that accommodated renewed strike-slip faulting (Figs. 21B and 21C), thus supporting an interpretation of full strain partitioning. Most of the initially steep strike-slip San Andreas fault strands, however, are now partly masked by fold-and-thrust structures (Fig. 21C). On the other hand, if most of the latest deformation in Mecca Hills is compressive, the bulk dextral motion along the San Andreas fault itself since the onset of transpressive deformation (<~4 m.y. ago) may have occurred during the first and second kinematic stages, at least locally (see discussion below).

Mechanisms of Transpressional Uplift Wedges

Classic positive flower structures form during simple shear transpressional deformation along restraining bends of a major, steep, strike-slip fault that underlies attendant wide zones of distributed en échelon folds and reverse faults oblique to the main fault (Wilcox et al., 1973; Sanderson and Marchini, 1984). The requisite condition for such a positive flower structure is that the master strike-slip fault and all related folds and reverse faults formed synchronously (Wilcox et al., 1973; Sylvester, 1988; Richard and Cobbold, 1990; Miller, 1998).

By contrast, more localized, narrow strike-slip fault zones and wider fault-parallel fold-and-thrust belts may form separately, during partitioned strain events (Harding, 1973; Wilcox, et al., 1973; Harding and Lowell, 1979; Mount and Suppe, 1987; Jones and Tanner, 1995; Miller, 1998). Ideal simple shear strain would result in a symmetrical, transpressional wedge or prism, or flower-like structure (Fig. 22A), whereas full strain partitioning in addition would result in a wedge-shaped or asymmetric prism (Figs. 22B and 22C) similar to that of contractile fold-and-thrust belt wedges (Dahlen, 1990; Koons, 1994; Leever et al., 2011a). In wedge-shaped partitioned shortening prisms (Fig. 22C), the highest and most uplifted part will abut a steep reverse or oblique strike-slip master fault, whereas gently dipping thrusts and related folds would form in the direction of tectonic transport, at high angle to the master fault (Fossen and Tikoff, 1993; Platt, 1993; Tikoff and Teyssier, 1994; Braathen et al., 1999; Leever et al., 2011a).

We propose a model in which the very complex, but still atypical flower-structure geometry of the Mecca Hills (Fig. 3) formed by polyphase deformation (Fig. 22). The evolution started with strike-slip–dominated distributed transpression and uplift of a near-symmetrical prism (Fig. 22A), and then switched to partly partitioned deformation (Fig. 22B), and ended with full strain partitioning, with growth of an asymmetric wedge-shaped shortening prism accommodating a frontal, SW-directed fold-and-thrust belt trending fully parallel to the San Andreas fault (Fig. 22C). In this model, the three-stage fold-fault structures were active in successive order (Fig. 21) and probably responded differently to changes in the uplifted wedges (cf. Braathen et al., 1999).

The increased degree of strain partitioning and topographic buildup in late kinematic stages (Figs. 22B and 22C) can be explained by progressive and/or renewed slip on a preexisting single, or branching, set of faults after sufficient uplift had occurred (Burbidge and Braun, 1998; Leever et al., 2011a), in order to maintain a critical wedge taper (Dahlen, 1990). Renewed slip transfer at constant plate obliquity, for example, would balance forces inside a transpressional uplift wedge (Dahlen, 1990) and lead to continued topographic uplift and erosion as inferred for the Mecca Hills (Sylvester, 1988; Dorsey et al., 2011; Fattaruso et al., 2014; Gray et al., 2014; McNabb et al., 2017).

Systematic reorientation of earlier-formed faults and/or resumed slip on new or favorably oriented adjacent faults could accommodate and adjust a symmetric transpressional uplift wedge to a stable critical taper (Davis et al., 1983; Dahlen, 1990). Similarly, a stable but asymmetric fold-and-thrust, shortening wedge taper may form by in-sequence, fold and fault propagation and frontal wedge imbrication, thus thickening and widening the wedge over time (Braathen et al., 1999). When an oversteepened, uplifted wedge geometry is achieved, however, a critical taper may be maintained by creating out-of-sequence thrusts, first in the interior of the wedge and then later at the frontal part of the wedge (cf. Dahlen, 1990). Such a hypothesis may explain how the Skeleton Canyon fault evolved from an initially steep, en échelon fault to a SW-directed out-of-sequence thrust, by renewed slip transfer in the late kinematic stage (Figs. 11, 21B, 21C, and 22C).

On a regional scale, the main controlling factors for transpressional uplift wedges and their further behavior are plate convergence angle, slip rates, and preexisting crustal structures (Richard and Cobbold, 1990; McClay et al., 2004). A convergence angle of ~8.4°, a 7:1 strike-slip to contraction ratio for the restraining bends in the Mecca Hills (Damte, 1997) and Durmid Hills (Bilham and Williams, 1985; Sylvester et al., 1993), and an ~5° plate obliquity have been calculated for central California (Argus and Gordon, 2001). This obliquity would favor lateral motion on a steep strike-slip fault (i.e., San Andreas fault) and distributed strain fields on either side of the fault (cf. Sanderson and Marchini, 1984; Mount and Suppe, 1987). The uplift and inversion of Mecca basin may therefore have been linked to an abrupt increase in plate obliquity (Lutz et al., 2006; Janecke et al., 2010) and/or local changes in partitioning of slip rates between the San Andreas fault and other faults (Bennett et al., 2004), e.g., in early Pleistocene time. Such changes would favor nucleation of steep strike-slip faults along preexisting, steep normal faults that bounded Mecca basin (Sylvester and Smith, 1987; Damte, 1997; McNabb et al., 2017), for example, the San Andreas fault and/or Painted Canyon fault (Sylvester and Smith, 1976). In this scenario, the result would be a distributed simple shear strain field with oblique folds and faults accompanied by near-symmetric uplift (Figs. 22A and 22B), and these structures then would have controlled further kinematic evolution and uplift in the Mecca Hills. A gradual switch to higher convergence angle, on the other hand, would result in increased shortening perpendicular to the San Andreas fault, strain partitioning (Mount and Suppe, 1987; Tikoff and Teyssier, 1994; Miller, 1998), and formation of an asymmetric wedge as during the second and third kinematic stages (Figs. 21B, 21C, and 22C).

In summary, the restraining bend structure of the San Andreas fault strand in the Mecca Hills was previously interpreted as a classic transpressional flower structure (Sylvester and Smith, 1976, 1987). We argue, however, that even though the final geometry of the San Andreas fault in Mecca Hills resembles that of a flower structure, it developed through a polyphase evolution of the San Andreas fault through a distributed to partitioned strain history. From our detailed field analysis in the Mecca Hills, and by comparing our data with physical and numerical models for transpressional deformation elsewhere along the San Andreas fault (Matti et al., 1992; Nicholson, 1996; Carena et al., 2004; Dair and Cooke, 2009; Cooke and Dair, 2011; Herbert and Cooke, 2012), we interpreted the parts of the flower structure that were active at each kinematic stage (Figs. 21 and 22). Our hypothesis is that distributed transpressional, partitioned strike-slip, and contractile structures formed successively to adjust the corresponding uplift shape or wedge to a critical taper (cf. Braathen et al., 1999). The overall result is that the initially steep San Andreas fault and subsequent en échelon folds are now mostly masked by an overlying, complex, decapitating surficial network of active, gently dipping fold-and-thrust systems (cf. Seeber and Armbruster, 1995; Yule, 2009).

Regional Implications

The Mecca Hills basin in Miocene–Pliocene time was part of a megascale supradetachment in the Salton Trough, divided by the steep master San Andreas

fault in the northwest and the gently dipping West Salton detachment to the south (Axen and Fletcher, 1998; Dorsey, 2006; Dorsey et al., 2011). The bounding normal fault of the Mecca basin (i.e., Painted Canyon fault) and most other extensional faults in the Mecca and Durmid Hills were all connected as listric faults to this detachment. New geophysical rotation data indicate Pacific plate motion became obliquely convergent with respect to the San Andreas fault of central California at ca. 5.2–4.2 Ma, in agreement with geologic evidence for a Pliocene onset of folding and faulting there (DeMets and Merkouvriev, 2016). Farther south, in mid-Pleistocene time, ca. 1.0 Ma, the entire Fish Creek–Valecito basin, including the Mecca Hills, and possibly also the Santa Rosa block deposits, started to rise and tilted northeast (Mason et al., 2017) due to a major tectonic reorganization that localized transpressive deformation to the northeast part of the Salton Trough and strike-slip deformation to the southwestern areas of Salton Trough (Matti and Morton, 1993; Morton and Matti, 1993; Janecke et al., 2010). This explanation is limited by the termination of slip on the West Salton detachment and initiation of the modern, still-active San Jacinto, San Felipe, and Elsinore strike-slip faults ca. 1.0 Ma (Lutz et al., 2006; Kirby et al., 2007; Steely et al., 2009; Janecke et al., 2010; Gray et al., 2014). Other reasons for this tectonic switch, such as regional crustal instabilities and/or a major change in the plate convergence angle, are unknown.

Strain-partitioning processes such as those inferred above along the San Andreas fault margin in the Mecca Hills through time have also been recognized elsewhere (e.g., Page, 1990; Page et al., 1998; Tavarnelli, 1998; Tavarnelli and Holdsworth, 1999). One possible explanation, however, for the very effective strain-partitioning kinematic behavior proposed for Mecca Hills resides in the recognition of the proto–San Andreas fault, which was active as a major facies boundary/normal fault since the Paleogene and later reactivated during the Miocene–Holocene time interval (cf. Nilsen, 1981; Page, 1990; Tavarnelli, 1998).

The first distributed deformation stage of the Mecca Hills basin (Fig. 22A) probably also affected other block-boundary fault zones and larger areas adjacent to the Mecca Hills (Fig. 3). For example, there is a direct linkage of the Skeleton Canyon fault with the San Andreas fault along restraining bends, and similar connections may exist with the Painted Canyon and Hidden Springs fault farther southeast (Fig. 2; Williams et al., 1990; Nicholson, 2009), thus facilitating reverse and/or lateral-slip displacement on these faults.

The second kinematic stage that reoriented en échelon folds to steeply plunging folds in the Basin block (Fig. 22B) is a unique record of a kinematic change to partitioned deformation that may have localized shear strain along the irregular, restraining-bend San Andreas fault–Basin block margin (cf. Miller, 1998). The fact that this reorientation occurred only in the Basin block suggests that most of the initial San Andreas fault–perpendicular shortening strain was localized on the San Andreas fault there. The data from Mecca Hills clearly suggest that deformation character changed through time, but this is not apparent for Durmid Hills, where the deformation is overall distributed and characterized by en échelon folds and folding of the Bishop Tuff (Bürgmann, 1991).

The latest kinematic stage in the Mecca Hills involved folding and SW-directed transport of thrust sheets that decapitated and masked the early San Andreas fault trace, and reshaped the Skeleton Canyon fault from a distributed strike-slip fault to a dominantly reverse, San Andreas fault–parallel fault. Similar, but opposite NE-directed reverse displacement occurred on the Painted Canyon fault along the northeast margin of the Platform block (Fig. 3). In this scenario, the Skeleton Canyon fault may have been reactivated as a temporally correlated, late-stage back-thrust relative to the Painted Canyon fault above a ramp below the Skeleton Canyon syncline in the Central block (Fig. 22C; Sylvester and Smith, 1976, 1987). This late kinematic stage marked a significant basement-seated uplift due to shortening along two or more oppositely dipping reverse faults, Skeleton Canyon and Painted Canyon faults, defining a crustal scale pop-up structure (Fig. 22C). This shortening model is supported by recent geophysical data (Nicholson, et al., 2015; Plesch, et al., 2015), which depict a NE-dipping fault system at depth, from which oblique-reverse strike-slip faults peel up to the surface. Those faults are young, represent shortening deformation, and include the Painted Canyon (i.e., Mecca Hills fault) and Hidden Springs faults.

Most of this uplift probably occurred in the late Pleistocene (<0.76 Ma), based on potential source data for the Ocotillo Formation in a dextral, transpressive setting. The lower part of the Ocotillo Formation exposed between Painted and Thermal Canyons and above the Bishop Tuff consists almost entirely of Orocopia Schist. Upward in the stratified sequence, the proportion of Orocopia Schist decreases relative to granite and gneiss. The nearest sources for sediment containing almost 100% schist are washes issuing out of the Orocopia Mountains, 15 km southeast of the Mecca Hills, which implies 15 km of right-slip displacement since deposition of the Bishop Tuff, 765,000 yr ago. The interpretation that strike-slip deformation continues today is supported by mechanical fault dip modeling (Fattaruso et al., 2014), quantitative geomorphic analysis (Gray et al., 2014), and documentation of ground-rupturing earthquakes along the San Andreas fault in the Salton Trough in the sixteenth and eighteenth centuries (Rockwell et al., 2018).

On the other hand, full strain partitioning during the last of the three stages requires the steep San Andreas fault to have acted as the through-going dextral strike-slip fault. However, significant dextral slip along the San Andreas fault cannot be demonstrated more recently than ca. 0.76 Ma, nor on nearby faults in the Mecca Hills. One option is that the Painted Canyon fault acted as a localized, steep dextral-oblique fault at the back side of the SW-directed fold-and-thrust belt wedge (Fig. 22C), yielding more cryptic dextral motion in the frontal areas. A second option is that slip partitioning occurred on a regional scale, i.e., dominantly shortening in Mecca Hills and dextral displacement transferred onto adjacent major strike-slip faults in Salton Trough like the San Jacinto, Elsinore, and/or San Felipe strike-faults farther west (Matti and Morton, 1993; Dorsey, 2006; Steely et al., 2009; Janecke et al., 2010; Fattaruso et al., 2014; Gray et al., 2014). This may have happened when the extensional West Salton detachment became inactive, which would have reduced the average dextral slip rate on the San Andreas fault (Janecke et al., 2010; Mason et al., 2017).

CONCLUSIONS

(1) In mid-Pleistocene time (1.0 Ma), the Mecca Hills transtensional basin, and its ~1300-m-thick Miocene and Pliocene sedimentary succession, was inverted, uplifted, and polyphase deformed, producing a complex transpressional uplift (wedge) between the bounding San Andreas fault and Painted Canyon fault. The resulting flower-like structure adjacent to the San Andreas fault core zone and off-fault deformation zone is expressed as en échelon folds and faults oblique to the San Andreas fault, steeply plunging folds, and San Andreas fault–parallel fold-and-thrust structures.

(2) The structural evolution started along a steep, localized San Andreas fault, followed by en échelon folding and faulting in a wide zone adjacent to the San Andreas fault, probably due to distributed simple shear strain. The subsidiary, right-lateral Skeleton Canyon fault formed along a restraining bend, and renewed right-lateral shearing along this fault reoriented the en échelon folds into steeply plunging folds almost parallel to the San Andreas fault, suggesting a switch from distributed to a localized partitioned strain field. The final stage produced wide SW-directed fold-and-thrust structures fully parallel to the San Andreas fault, which were emplaced upon, and decapitated previously formed, structures within a fully partitioned, but dominantly shortening strain field. Our model maintains that the initial Skeleton Canyon fault reactivated as a back-thrust above a thrust ramp relative to the reverse, Painted Canyon boundary fault of the Mecca basin farther northeast. The strike-slip component of the partitioned strain field was either transferred onto steep, nearby en échelon or oblique-reverse faults in the Mecca Hills, or onto still-active, regional-scale, strike-slip faults in the Salton Trough of southern California.

(3) The polyphase kinematic evolution from distributed to partitioned strain domains across and along strike of the San Andreas fault in the Mecca Hills could reflect a small change in plate convergence angle, but it more likely reflects a local change in crustal rheology. In the latter case, if an oversteepened transpressional wedge had formed during the early, distributed stage, then geometric adjustment to a lower taper angle would have been achieved by in-sequence and then break-back fold-and-thrust displacement on renewed, previously formed steep faults, e.g., Skeleton Canyon and/or Painted Canyon faults. The late-stage partitioned model with dominant San Andreas fault–perpendicular shortening thus explains why the Mecca Hills are still undergoing fault-controlled uplift and considerable erosion. One possible explanation for the very effective strain-partitioning and kinematic behavior as documented in Mecca Hills resides in the recognition of a proto–San Andreas fault that was active as a major facies boundary/normal fault since Paleogene time.

(4) The kinematic model for the Mecca Hills may be of broad interest and scientific significance because it explains how the classical model of a flower structure geometry, in which all structures form synchronously (Sylvester and Smith, 1976, 1987), needs to be updated to the more nuanced view of a polyphase system. Our data and field approach clearly indicate the need to carefully sort out spatially and temporally different structural and kinematic data as a basis for analog and numerical modeling of transpressional uplift areas.

ACKNOWLEDGMENTS

Bergh thanks the staff at the University of California–Santa Barbara (UCSB) and San Diego State University for great hospitality during his sabbatical leaves in 2011–2012 and 2016–2017, respectively, while working with the San Andreas fault. Funding was provided by grants from the University of Tromsø–The Arctic University of Norway and the National Research Foundation of Norway. Reviewers Gary Axen, Basil Tikoff, and Enrico Tavarnelli provided constructive comments that greatly improved the paper. Sylvester acknowledges a travel grant from the UCSB Academic Senate. Publication charges have been funded by grants from the publication fund of UiT The Arctic University of Norway, and from an ARCEx-UiT project studying analogue transform faults to Svalbard and Barents Sea.

REFERENCES CITED

Aleksandrowski, P., 1985, Graphical determination of principal stress directions for slickenside lineation populations: An attempt to modify Arthaud's method: Journal of Structural Geology, v. 7, p. 73–82, https://doi.org/10.1016/0191-8141(85)90116-6.

Argus, D.F., and Gordon, R.G., 2001, Present tectonic motion across the Coast Ranges and San Andreas fault system in central California: Geological Society of America Bulletin, v. 113, no. 12, p. 1580–1592, https://doi.org/10.1130/0016-7606(2001)113<1580:PTMATC>2.0.CO;2.

Atwater, T., and Stock, J.M., 1998, Pacific–North America plate tectonics of the Neogene southwestern United States: An update: International Geology Review, v. 40, no. 5, p. 375–402, https://doi.org/10.1080/00206819809465216.

Axen, G.J., and Fletcher, J.M., 1998, Late Miocene–Pleistocene extensional faulting, northern Gulf of California, Mexico, and Salton Trough, California: International Geology Review, v. 40, p. 217–244, https://doi.org/10.1080/00206819809465207.

Babcock, E.A., 1974, Geology of the northeast margin of the Salton Trough, Salton Sea, California: Geological Society of America Bulletin, v. 85, p. 321–332, https://doi.org/10.1130/0016-7606(1974)85<321:GOTNMO>2.0.CO;2.

Bally, A.W., Gordy, P.L., and Stewart, G.A., 1966, Structure, seismic data, and orogenic evolution of southern Canadian Rocky Mountains: Bulletin of Canadian Petroleum Geology, v. 14, no. 3, p. 337–381.

Bennett, R.A., Friedrich, A.M., and Furlong, K.P., 2004, Co-dependent histories of the San Andreas and San Jacinto fault zones from inversion of fault displacement rates: Geology, v. 32, p. 961–964, https://doi.org/10.1130/G20806.1.

Bergh, S.G., and Grogan, P., 2003, Tertiary structure of the Sørkapp-Hornsund region, south Spitsbergen, and implications for the offshore southern extension of the fold-thrust belt: Norsk Geologisk Tidsskrift, v. 83, no. 1, p. 43–60.

Bergh, S.G., Braathen, A., and Andresen, A., 1997, Interaction of basement-involved and thin-skinned tectonism in the Tertiary fold-and thrust belt of central Spitsbergen, Svalbard: American Association of Petroleum Geologists Bulletin, v. 81, p. 637–661.

Bergh, S.G., Maher, H.D., Jr., and Braathen, A., 2000, Tertiary divergent thrust directions from partitioned transpression, Brøggerhalvøya, Spitsbergen: Norsk Geologisk Tidsskrift, v. 80, p. 63–81, https://doi.org/10.1080/002919600750042573.

Bergh, S.G., Kullerud, K., Armitage, P.E.B., Zwaan, K.B., Corfu, F., Ravna, E.J.K., and Myhre, P.I., 2010, Neoarchaean to Svecofennian tectono-magmatic evolution of the West Troms basement complex, North Norway: Norsk Geologisk Tidsskrift, v. 90, p. 21–48.

Bilham, R., and Williams, P., 1985, Sawtooth segmentation and deformation processes on the southern San Andreas fault, California: Geophysical Research Letters, v. 12, p. 557–560, https://doi.org/10.1029/GL012i009p00557.

Boley, J.-L., Stimac, J.P., Weldon, R.J., II, and Rymer, M.J., 1994, Stratigraphy and paleomagnetism of the Mecca and Indio Hills, southern California, *in* McGill, S.F., and Ross, T.M., eds., Geological Investigations of an Active Margin: Geological Society of America, Cordilleran

Section Guidebook, 27th Annual Meeting: San Bernardino, California, San Bernardino County Museum Association, p. 336–344.
Boyer, S.E., and Elliott, D., 1982, Thrust systems: American Association of Petroleum Geologists Bulletin, v. 66, p. 1196–1230.
Braathen, A., Bergh, S.G., and Maher, H.D., Jr., 1999, Application of a critical wedge taper model to the Tertiary transpressional fold-thrust belt on Spitsbergen, Svalbard: Geological Society of America Bulletin, v. 111, p. 1468–1485, https://doi.org/10.1130/0016-7606(1999)111<1468:AOACWT>2.3.CO;2.
Braun, J., and Beaumont, C., 1995, Three-dimensional numerical experiments of strain partitioning at oblique plate boundaries: Implications for contrasting tectonic styles in the southern Coast Ranges, California, and central South Island, New Zealand: Journal of Geophysical Research, v. 100, no. B9, p. 18,059–18,074, https://doi.org/10.1029/95JB01683.
Burbidge, D.R., and Braun, J., 1998, Analogue models of obliquely convergent continental plate boundaries: Journal of Geophysical Research, v. 103, no. B7, p. 15,221–15,237, https://doi.org/10.1029/98JB00751.
Bürgmann, R., 1991, Transpression along the southern San Andreas fault, Durmid Hill, California: Tectonics, v. 10, p. 1152–1163, https://doi.org/10.1029/91TC01443.
Butler, R.W.H., 1982, The terminology of structures in thrust belts: Journal of Structural Geology, v. 4, no. 3, p. 239–245, https://doi.org/10.1016/0191-8141(82)90011-6.
Butler, R.W.H., 1987, Thrust sequences: Journal of the Geological Society [London], v. 144, p. 619–634, https://doi.org/10.1144/gsjgs.144.4.0619.
Carena, S., Suppe, J., and Kao, H., 2004, Lack of continuity of the San Andreas fault in southern California: Three-dimensional fault models and earthquake scenarios: Journal of Geophysical Research–Solid Earth, v. 109, no. B4, B04313, https://doi.org/10.1029/2003JB0022643.
Chang, S.-B.R., Allen, C.R., and Kirschvink, J.L., 1987, Magnetic stratigraphy and a test for block rotation of sedimentary rocks within the San Andreas fault zone, Mecca Hills, southeastern California: Quaternary Research, v. 27, p. 30–40, https://doi.org/10.1016/0033-5894(87)90047-0.
Cooke, M.L., and Dair, L., 2011, Simulating the recent evolution of the southern big bend of the San Andreas fault, southern California: Journal of Geophysical Research, v. 116, B04405, https://doi.org/10.1029/2010JB007835.
Crowell, J.C., 1981, An outline of the tectonic history of southeastern California, *in* Ernst, W.G., ed., The Geotectonic Development of California: Rubey Volume 1: Englewood Cliffs, New Jersey, Prentice-Hall, p. 583–600.
Crowell, J.C., and Sylvester, A.G., eds., 1979, Tectonics of the Junction between the San Andreas Fault System and the Salton Trough, Southeastern California—Guidebook: Santa Barbara, California, Department of Geological Sciences, University of California–Santa Barbara, 193 p.
Dahlen, F.A., 1990, Critical taper model of fold-and-thrust belts and accretionary wedges: Annual Review of Earth and Planetary Sciences, v. 18, p. 55–99, https://doi.org/10.1146/annurev.ea.18.050190.000415.
Dair, L., and Cooke, M.L., 2009, San Andreas fault geometry through the San Gorgonio Pass, California: Geology, v. 37, p. 119–122, https://doi.org/10.1130/G25101A.1.
Dallmann, W.K., Andresen, A., Bergh, S.G., Maher, H.D., Jr., and Ohta, Y., 1993, Tertiary fold-and-thrust belt of Spitsbergen, Svalbard: Compilation map, summary, and bibliography: Norsk Polarinstitutt Report, v. 128, p. 1–46.
Damte, A., 1997, Styles of Deformation in Zones of Oblique Convergence: Example from Mecca Hills, Southern San Andreas Fault [PhD thesis]: Santa Barbara, California, University of California, 164 p.
Damte, A., and Biehler, S., 1995, Gravity modeling of the basement surface in the Mecca Hills, southern San Andreas fault [abs.]: American Geophysical Union Transactions, v. 76, p. F597.
Davis, D., Suppe, J., and Dahlen, F.A., 1983, Mechanics of fold-and-thrust belts and accretionary wedges: Journal of Geophysical Research, v. 88, no. B2, p. 1153–1172, https://doi.org/10.1029/JB088iB02p01153.
DeMets, C., and Merkouriev, S., 2016, High-resolution reconstructions of Pacific–North America plate motion: 20 Ma to present: Geophysical Journal International, v. 207, p. 741–773, https://doi.org/10.1093/gji/ggw305.
Dewey, J.E., Holdsworth, R.E., and Strachan, R.A., 1998, Transpression and transtension zones, *in* Holdsworth, R.E., Strachan, R.A., and Dewey, J.E., eds., Continental Transpressional and Transtensional Tectonics: Geological Society [London] Special Publication 135, p. 1–14.
Dibblee, T.W., Jr., 1954, Geology of the Imperial Valley region, California, *in* Jahns, R.H., ed., Geology of Southern California: California Division of Mines Bulletin 170, p. 21–28.
Dibblee, T.W., Jr., 1984, Stratigraphy and tectonics of the San Felipe Hills, Borrego Badlands, Superstition Hills, and vicinity, *in* Rigsby, C.A., ed., The Imperial Basin—Tectonics, Sedimentation, and Thermal Aspects: Los Angeles, California, Pacific Section, Society of Economic Paleontologists and Mineralogists (SEPM), p. 31–44.
Dolan, J.F., Bowman, D.D., and Sammis, C.G., 2007, Long-range and long-term fault interactions in southern California: Geology, v. 35, no. 9, p. 855–858, https://doi.org/10.1130/G23789A.1.
Dorsey, R.J., 2006, Stratigraphy, tectonics, and basin evolution in the Anza-Borrego Desert region, *in* Jefferson, G.T., and Lindsay, L.E., eds., Fossil Treasures of Anza-Borrego Desert: San Diego, California, Sunbelt Publications, p. 89–104.
Dorsey, R.J., Housen, B.A., Janecke, S.U., Fanning, C.M., and Spears, A.L.F., 2011, Stratigraphic record of basin development within the San Andreas fault system: Late Cenozoic Fish Creek–Vallecito basin, southern California: Geological Society of America Bulletin, v. 123, p. 771–793, https://doi.org/10.1130/B30168.1.
Dunne, W.M., and Hancock, P.L., 1994, Paleostress analysis of small-scale brittle structures, *in* Hancock, P.L., ed., Continental Deformation: Oxford, UK, Pergamon Press, p. 101–120.
Erslev, E.A., 1991, Trishear fault-propagation folding: Geology, v. 19, no. 6, p. 617–620, https://doi.org/10.1130/0091-7613(1991)019<0617:TFPF>2.3.CO;2.
Fattaruso, L.A., Cooke, M.L., and Dorsey, R.J., 2014, Sensitivity of uplift patterns to dip of the San Andreas fault in the Coachella Valley, California: Geosphere, v. 10, p. 1235–1246, https://doi.org/10.1130/GES01050.1.
Fossen, H., and Tikoff, B., 1993, The deformation matrix for simultaneous simple shearing, pure shearing, and volume change, and its application to transpression/transtension tectonics: Journal of Structural Geology, v. 15, no. 3–5, p. 413–422, https://doi.org/10.1016/0191-8141(93)90137-Y.
Fossen, H., Tikoff, B., and Teyssier, C., 1994, Strain modeling of transpressional and transtensional deformation: Norsk Geologisk Tidsskrift, v. 74, p. 134–145.
Frost, E.G., and Martin, D.L., eds., 1982, Mesozoic–Cenozoic Tectonic Evolution of the Colorado River Region, California, Arizona, and Nevada: Anderson-Hamilton Volume: San Diego, California, Cordilleran Publishers, 608 p.
Fuis, G.S., and Kohler, W.M., 1984, Crustal structure and tectonics of the Imperial Valley region, California, *in* Rigsby, C.S., ed., The Imperial Basin—Tectonics, Sedimentation, and Thermal Aspects: Los Angeles, California, Pacific Section, Society of Economic Paleontologists and Mineralogists (SEPM), p. 1–13.
Garde, A.A., Chadwick, B., Grocott, J., Hamilton, M.A., McCaffrey, K.J.W., and Swager, C.P., 2002, Mid-crustal partitioning and attachment during oblique convergence in an arc system, Palaeoproterozoic Ketilidian orogen, southern Greenland: Journal of the Geological Society [London], v. 159, p. 247–261, https://doi.org/10.1144/0016-764901-080.
Gray, H.J., Owen, L.A., Dietsch, C., Beck, R.A., Caffee, M.A., Finkel, R.C., and Mahan, S.A., 2014, Quaternary landscape development, alluvial fan chronology and erosion of the Mecca Hills at the southern end of the San Andreas fault zone: Quaternary Science Reviews, v. 105, p. 66–85, https://doi.org/10.1016/j.quascirev.2014.09.009.
Hamilton, W., 1961, Origin of the Gulf of California: Geological Society of America Bulletin, v. 72, p. 1307–1318, https://doi.org/10.1130/0016-7606(1961)72[1307:OOTGOC]2.0.CO;2.
Hamilton, W., and Myers, W.B., 1966, Cenozoic tectonics of the western United States: Reviews of Geophysics, v. 4, p. 509–549, https://doi.org/10.1029/RG004i004p00509.
Hancock, P.L., 1985, Brittle microtectonics: Principles and practice: Journal of Structural Geology, v. 7, p. 437–457, https://doi.org/10.1016/0191-8141(85)90048-3.
Harding, T.P., 1973, Newport-Inglewood trend, California—An example of wrenching style of deformation: American Association of Petroleum Geologists Bulletin, v. 57, no. 1, p. 97–116.
Harding, T.P., and Lowell, J.D., 1979, Structural styles, their plate tectonic habitats, and hydrocarbon traps in petroleum provinces: American Association of Petroleum Geologists Bulletin, v. 63, p. 1016–1058.
Harland, W.B., 1971, Tectonic transpression in Caledonian Spitsbergen: Geological Magazine, v. 108, p. 27–42, https://doi.org/10.1017/S0016756800050937.
Herbert, J.W., and Cooke, M.L., 2012, Sensitivity of the southern San Andreas fault system to tectonic boundary conditions and fault configurations: Bulletin of the Seismological Society of America, v. 102, no. 5, p. 2046–2062, https://doi.org/10.1785/0120110316.
Herzig, C.T., and Jacobs, D.C., 1994, Cenozoic volcanism and two-stage extension in the Salton Trough, southern California and northern Baja California: Geology, v. 22, no. 11, p. 991–994, https://doi.org/10.1130/0091-7613(1994)022<0991:CVATSE>2.3.CO;2.
Herzig, C.T., Mehegan, J.M., and Stelting, C.E., 1988, Lithostratigraphy of the State 2–14 borehole: Salton Sea Scientific Drilling Project: Journal of Geophysical Research–Solid Earth, v. 93, no. B11, p. 12,969–12,980, https://doi.org/10.1029/JB093iB11p12969.

Holdsworth, R.E., Tavarnelli, E., Clegg, P., Pinheiro, R.V., Jones, R.R., and McCaffrey, K.J.W., 2002, Domainal deformation patterns and strain partitioning during transpression: An example from the Southern Uplands, Scotland: Journal of the Geological Society [London], v. 159, p. 401–415, https://doi.org/10.1144/0016-764901-123.

Hulen, J.B., and Pulka, F.S., 2001, Newly discovered, ancient extrusive rhyolite in the Salton Sea geothermal field, Imperial Valley, California: Implications for reservoir characterization and duration of volcanism in the Salton Trough, *in* Proceedings of the Twenty-Sixth Workshop on Geothermal Reservoir Engineering, January 29–31, 2001: Stanford, California, Stanford University, SGP-TR-168.

Ingersoll, R.V., and Rumelhart, P.E., 1999, Three-stage evolution of the Los Angeles Basin, southern California: Geology, v. 27, p. 593–596, https://doi.org/10.1130/0091-7613(1999)027<0593:TSEOTL>2.3.CO;2.

Jamison, W.R., 1987, Geometric analysis of fold development in overthrust terranes: Journal of Structural Geology, v. 9, p. 207–219, https://doi.org/10.1016/0191-8141(87)90026-5.

Jamison, W.R., 1991, Kinematics of compressional fold development in convergent wrench terranes: Tectonophysics, v. 190, p. 209–232, https://doi.org/10.1016/0040-1951(91)90431-Q.

Janecke, S.U., Dorsey, R.J., Forand, D., Steely, A.N., Kirby, S.M., Lutz, A.T., Housen, B.A., Belgarde, B., Langenheim, V.E., and Rittenour, T.M., 2010, High geologic slip rates since early Pleistocene initiation of the San Jacinto and San Felipe fault zone in the San Andreas fault system, southern California, USA: Geological Society of America Special Paper 475, 48 p., https://doi.org/10.1130/2010.2475.

Jones, R.R., and Tanner, P.W.G., 1995, Strain partitioning in transpression zones: Journal of Structural Geology, v. 17, p. 793–802, https://doi.org/10.1016/0191-8141(94)00102-6.

Jones, R.R., Holdsworth, R.E., and Bailey, W., 1997, Lateral extrusion in transpression zones: The importance of boundary conditions: Journal of Structural Geology, v. 19, p. 1201–1217, https://doi.org/10.1016/S0191-8141(97)00034-5.

Jones, R.R., Holdsworth, R.H., Clegg, P., McCaffrey, K., and Tavarnelli, E., 2004, Inclined transpression: Journal of Structural Geology, v. 26, p. 1531–1548, https://doi.org/10.1016/j.jsg.2004.01.004.

Keller, E.A., Bonkowski, M.S., Korsch, R.J., and Shlemon, R.J., 1982, Tectonic geomorphology of the San Andreas fault zone in the southern Indio Hills, Coachella Valley, California: Geological Society of America Bulletin, v. 93, p. 46–56, https://doi.org/10.1130/0016-7606(1982)93<46:TGOTSA>2.0.CO;2.

Kirby, S.M., Janecke, S.U., Dorsey, R.J., Housen, B.A., McDougall, K., Langenheim, V., and Steely, A., 2007, Pleistocene Brawley and Ocotillo Formations: Evidence for initial strike-slip deformation along the San Felipe and San Jacinto fault zones, California: The Journal of Geology, v. 115, p. 43–62, https://doi.org/10.1086/509248.

Koons, P.O., 1994, Three-dimensional critical wedges: Tectonics and topography in oblique collisional orogens: Journal of Geophysical Research, v. 99, no. B6, p. 12,301–12,315, https://doi.org/10.1029/94JB00611.

Leever, K.A., Gabrielsen, R.H., Sokoutis, D., and Willingshofer, E., 2011a, The effect of convergence angle on the kinematic evolution of strain partitioning in transpressional brittle wedges: Insight from analog modeling and high-resolution digital image analysis: Tectonics, v. 30, TC2013, https://doi.org/10.1029/2010TC002823.

Leever, K.A., Gabrielsen, R.H., Faleide, J.I., and Braathen, A., 2011b, A transpressional origin for the West Spitsbergen fold-and-thrust belt: Insight from analog modeling: Tectonics, v. 30, TC2014, https://doi.org/10.1029/2010TC002753.

Lutz, A.T., Dorsey, R.J., Housen, B.A., and Janecke, S.U., 2006, Stratigraphic record of Pleistocene faulting and basin evolution in the Borrego Badlands, San Jacinto fault zone, southern California: Geological Society of America Bulletin, v. 118, p. 1377–1397, https://doi.org/10.1130/B25946.1.

Maher, H.D., Jr., and Craddock, C., 1988, Decoupling as an alternative model for transpression during the initial opening of the Norwegian-Greenland Sea: Polar Research, v. 6, p. 137–140, https://doi.org/10.3402/polar.v6i1.6855.

Maher, H.D., Jr., Braathen, A., Bergh, S.G., Dallmann, W.K., and Harland, W.B., 1995, Tertiary or Cretaceous age for Spitsbergen's fold-thrust belt on the Barents Shelf?: Tectonics, v. 14, no. 6, p. 1321–1326, https://doi.org/10.1029/95TC01257.

Mason, C.C., Spotila, J.A., Axen, G., Dorsey, R.J., Luther, A., and Stockli, D.F., 2017, Two-phase exhumation of the Santa Rosa Mountains: Low- and high-angle normal faulting during initiation and evolution of the southern San Andreas fault system: Tectonics, v. 36, p. 2863–2881, https://doi.org/10.1002/2017TC004498.

Matti, J.C., and Morton, D.M., 1993, Paleogeographic evolution of the San Andreas fault in southern California: A reconstruction based on a new cross-fault correlation, *in* Powell, R.E., Weldon, R.J., II, and Matti, J.C., eds., The San Andreas Fault System: Displacement, Palinspastic Reconstruction, and Geological Evolution: Geological Society of America Memoir 178, p. 107–160, https://doi.org/10.1130/MEM178-p107.

Matti, J.C., Morton, D.M., and Cox, B.F., 1992, The San Andreas Fault System in the Vicinity of the Central Transverse Ranges Province, Southern California: U.S. Geological Survey Open-File Report 92–354, 49 p.

McCaffrey, K.J.W., 1992, Igneous emplacement in a transpressive shear zone: Ox Mountains igneous complex: Journal of the Geological Society [London], v. 149, no. 2, p. 221–235, https://doi.org/10.1144/gsjgs.149.2.0221.

McClay, K., and Bonora, M., 2001, Analog models of restraining stepovers in strike-slip fault systems: American Association of Petroleum Geologists Bulletin, v. 85, p. 233–260.

McClay, K.R., Whitehouse, P.S., Dooley, T., and Richards, M., 2004, 3D evolution of fold and thrust belts formed by oblique convergence: Marine and Petroleum Geology, v. 21, no. 7, p. 857–877, https://doi.org/10.1016/j.marpetgeo.2004.03.009.

McNabb, J.C., Dorsey, R.J., Housen, B.A., Dimitroff, C.W., and Messé, G.T., 2017, Stratigraphic record of Pliocene–Pleistocene basin evolution and deformation with the southern San Andreas fault zone, Mecca Hills, California: Tectonophysics, v. 719–720, p. 66–85, https://doi.org/10.1016/j.tecto.2017.03.021.

Miller, D.D., 1998, Distributed shear, rotation, and partitioned strain along the San Andreas fault, central California: Geology, v. 26, no. 10, p. 867–870, https://doi.org/10.1130/0091-7613(1998)026<0867:DSRAPS>2.3.CO;2.

Molinaro, M., Leturmy, P., Guezou, J.-C., Frizon de Lamotte, D., and Eshraghi, S.A., 2005, The structure and kinematics of the southeastern Zagros fold-thrust belt, Iran: From thin-skinned to thick-skinned tectonics: Tectonics, v. 24, TC3007, https://doi.org/10.1029/2004TC001633.

Morley, C.K., 1988, Out-of-sequence thrusts: Tectonics, v. 7, p. 539–561, https://doi.org/10.1029/TC007i003p00539.

Morton, D.M., and Matti, J.C., 1993, Extension and contraction within an evolving divergent strike-slip fault complex: The San Andreas and San Jacinto fault zones at their convergence in southern California, *in* Powell, R.E., Weldon, R.J., II, and Matti, J.C., eds., The San Andreas Fault System: Displacement, Palinspastic Reconstruction, and Geologic Evolution: Geological Society of America Memoir 178, p. 217–230, https://doi.org/10.1130/MEM178-p217.

Mount, V.S., and Suppe, J., 1987, State of stress near the San Andreas fault: Implications for wrench tectonics: Geology, v. 15, p. 1143–1146, https://doi.org/10.1130/0091-7613(1987)15<1143:SOSNTS>2.0.CO;2.

Nicholson, C., 1996, Seismic behavior of the San Andreas fault in the northern Coachella Valley, California: Comparison of the 1948 and 1986 earthquake sequences: Bulletin of the Seismological Society of America, v. 86, p. 1331–1349.

Nicholson, C., 2009, Helping to Evaluate and Improve the SCEC 3D Community Fault Model and Regional Seismicity Catalogs: 2008 Southern California Earthquake Center Annual Report 08122, 7 p.

Nicholson, C., Sorlien, C.C., Atwater, T., Crowell, J.C., and Luyendyk, B.P., 1994, Microplate capture, rotation of the western Transverse Ranges, and initiation of the San Andreas transform as a low-angle fault system: Geology, v. 22, p. 491–495, https://doi.org/10.1130/0091-7613(1994)022<0491:MCROTW>2.3.CO;2.

Nicholson, C., Plesch, A., Sorlien, C.C., Shaw, J.H., and Hauksson, E., 2015, The SCEC Community Fault Model Version 5.0: An Updated and Expanded 3D Fault Set for Southern California: 2015 Pacific Section American Association of Petroleum Geologists Joint Meeting Program: Oxnard, California, American Association of Petroleum Geologists, 77 p.

Nilsen, T.H., 1981, Late Cretaceous geology of California and the problem of the proto–San Andreas fault, *in* Howell, D.G., and McDougall, K.A., eds., Mesozoic Palaeogeography of the Western United States: Los Angeles, California, Pacific Section, Society of Economic Paleontologists and Mineralogists (SEPM), Pacific Coast Paleogeography Symposium 2, p. 559–573.

Oldow, J.S., Bally, A.W., and Lallémant, H.G.A., 1990, Transpression, orogenic float, and lithospheric balance: Geology, v. 18, no. 10, p. 991–994, https://doi.org/10.1130/0091-7613(1990)018<0991:TOFALB>2.3.CO;2.

Oskin, M., and Stock, J.M., 2003, Marine incursion synchronous with plate boundary localization in the Gulf of California: Geology, v. 31, no. 1, p. 23–26, https://doi.org/10.1130/0091-7613(2003)031<0023:MISWPB>2.0.CO;2.

Page, B.M., 1990, Evolution and complexities of the transform system in California, U.S.A.: Annales Tectonicae, special issue, supplement to v. 4, p. 53–69.

Page, B.M., Thompson, G.A., and Coleman, R.G., 1998, Late Cenozoic tectonics of the central and southern Coast Ranges of California: Geological Society of America Bulletin, v. 110, p. 846–876, https://doi.org/10.1130/0016-7606(1998)110<0846:OLCTOT>2.3.CO;2.

Platt, J.P., 1993, Mechanics of oblique convergence: Journal of Geophysical Research, v. 98, p. 16,239–16,256, https://doi.org/10.1029/93JB00888.
Plesch, A., Shaw, J.H., Nicholson, C., Sorlien, C.C., and Statewide Community Fault Model Workshop Participants, 2015, Release and Evaluation of the Statewide Community Fault Model (SCFM) Version 3.0 and Continued Updates to the SCEC CFM 5.0, *in* 2015 Southern California Earthquake Center Annual Meeting Proceedings & Abstracts XXV: Southern California Earthquake Center, poster 217, p. 175.
Price, R.A., 1986, The southeastern Canadian Cordillera: Thrust faulting, tectonic wedging, and delamination of the lithosphere: Journal of Structural Geology, v. 8, p. 239–254, https://doi.org/10.1016/0191-8141(86)90046-5.
Reches, Z., 1978, Analysis of faulting in three-dimensional strain field: Tectonophysics, v. 47, p. 109–129, https://doi.org/10.1016/0040-1951(78)90154-3.
Richard, P.D., and Cobbold, P.R., 1990, Experimental insights into partitioning of fault motions in continental convergent wrench zones: Annales Tectonicae, v. 4, p. 35–44.
Richard, P.D., Mocquet, B., and Cobbold, P.R., 1991, Experiments on simultaneous faulting and folding above a basement wrench fault: Tectonophysics, v. 188, p. 133–141, https://doi.org/10.1016/0040-1951(91)90319-N.
Robinson, P.T., Elders, W.A., and Muffler, L.P.J., 1976, Quaternary volcanism in the Salton Sea geothermal field, Imperial Valley, California: Geological Society of America Bulletin, v. 87, no. 3, p. 347–360, https://doi.org/10.1130/0016-7606(1976)87<347:QVITSS>2.0.CO;2.
Rockwell, T.K., Meltzner, A.J., and Haaker, E.C., 2018, Dates of the two most recent surface ruptures on the southernmost San Andreas fault recalculated by precise dating of Lake Cahuilla dry periods: Bulletin of the Seismological Society of America, v. 108, no. 5A, p. 2634–2649, https://doi.org/10.1785/0120170392.
Rowe, C.D., and Griffith, W.A., 2015, Do faults preserve a record of seismic slip? A second opinion: Journal of Structural Geology, v. 78, p. 1–26, https://doi.org/10.1016/j.jsg.2015.06.006.
Sanderson, D.J., and Marchini, W.R.D., 1984, Transpression: The Journal of Geology, v. 6, p. 449–458.
Saucier, F., Humphreys, E., and Weldon, R.J., II, 1992, Stress near geometrically complex strike-faults: Application to the San Andreas fault at Cajon Pass, southern California: Journal of Geophysical Research, v. 97, p. 5081–5094, https://doi.org/10.1029/91JB02644.
Schreurs, G., and Colletta, B., 1998, Analogue modeling of faulting in zones of continental transpression and transtension, *in* Holdsworth, R.E., Strachan, R.A., and Dewey, J.F., eds., Continental Transpressional and Transtensional Tectonics: Geological Society, London, Special Publication 135, p. 59–79, https://doi.org/10.1144/GSL.SP.1998.135.01.05.
Seeber, L., and Armbruster, J.G., 1995, The San Andreas fault system through the Transverse Ranges as illuminated by earthquakes: Journal of Geophysical Research–Solid Earth, v. 100, no. B5, p. 8285–8310, https://doi.org/10.1029/94JB02939.
Sheridan, J.M., and Weldon, R.J., II, 1994, Accommodation of compression in the Mecca Hills, California, *in* McGill, S.F., and Ross, T.M., eds., Geological Investigations of an Active Margin: Guidebook: Redlands, California, Geological Society of America, Cordilleran Section, San Bernardino County Museum, p. 330–336.
Shirvell, C.R., Stockli, D.F., Axen, G.J., and Grove, M., 2009, Miocene–Pliocene exhumation along the West Salton detachment fault, southern California, from (U-Th)/He thermochronometry of apatite and zircon: Tectonics, v. 28, TC2006, https://doi.org/10.1029/2007TC002172.
Sieh, K.E., and Jahns, R.H., 1984, Holocene activity of the San Andreas fault at Wallace Creek, California: Geological Society of America Bulletin, v. 95, p. 883–896, https://doi.org/10.1130/0016-7606(1984)95<883:HAOTSA>2.0.CO;2.
Spotila, J.A., House, M.A., Niemi, N.A., Brady, R.C., Oskin, M., and Buscher, J.T., 2007, Patterns of bedrock uplift along the San Andreas fault and implications for mechanisms of transpression, *in* Till, A.B., Roeske, S.M., Sample, J.C., and Foster, D.A., eds., Exhumation Associated with Continental Strike-Slip Fault Systems: Geological Society of America Special Paper 434, p.15–33, https://doi.org/10.1130/2007.2434(02).
Stearns, D.W., 1968, Faulting and forced folding in the Rocky Mountains foreland, *in* Matthews, W., ed., Laramide Folding Associated with Basement Block Faulting in the Western United States: Geological Society of America Memoir 151, p. 1–37.
Steely, A.N., Janecke, S.U., Dorsey, R.J., and Axen, G.J., 2009, Early Pleistocene initiation of the San Felipe fault zone, SW Salton Trough, during reorganization of the San Andreas fault system: Geological Society of America Bulletin, v. 121, p. 663–687, https://doi.org/10.1130/B26239.1.
Stock, J.M., and Hodges, K.V., 1989, Pre-Pliocene extension around the Gulf of California and the transfer of Baja California to the Pacific plate: Tectonics, v. 8, p. 99–115, https://doi.org/10.1029/TC008i001p00099.
Sylvester, A.G., 1988, Strike-slip faults: Geological Society of America Bulletin, v. 100, p. 1666–1703.
Sylvester, A.G., and O'Black Gans, E., 2016, Roadside Geology of Southern California: Missoula, Montana, Mountain Press Publishing Company, 390 p.
Sylvester, A.G., and Smith, R.R., 1976, Tectonic transpression and basement-controlled deformation in the San Andreas fault zone, Salton Trough, California: American Association of Petroleum Geologists Bulletin, v. 60, p. 2081–2102.
Sylvester, A.G., and Smith, R.R., 1987, Structure section in Painted Canyon, Mecca Hills, southern California, *in* Hill, M.L., ed., Cordilleran Section, Geological Society of America Field Guide, p. 103–108.
Sylvester, A.G., Bilham, R., Jackson, M., and Barrientos, S., 1993, Aseismic growth of Durmid Hill, southeasternmost San Andreas fault, California: Journal of Geophysical Research, v. 98, p. 14,233–14,243, https://doi.org/10.1029/93JB01028.
Tavarnelli, E., 1998, Tectonic evolution of the Northern Salinian block, California, USA: Palaeogene-to-Recent shortening in a transform fault–bounded continental fragment, *in* Holdsworth R.E., Strachan, R., and Dewey, J.F., eds., Continental Transpressional and Transtensional Tectonics: Geological Society, London, Special Publication 135, p. 107–118, https://doi.org/10.1144/GSL.SP.1998.135.01.07.
Tavarnelli, E., and Holdsworth, R.E., 1999, How long do structures take to form in transpression zones? A cautionary tale from California: Geology, v. 27, p. 1063–1066, https://doi.org/10.1130/0091-7613(1999)027<1063:HLDSTT>2.3.CO;2.
Tavarnelli, E., and Pasqui, V., 2000, Fault growth by segment linkage in seismically active settings: Examples from the Southern Apennines, Italy, and the Coast Ranges, California: Journal of Geodynamics, v. 29, p. 501–516, https://doi.org/10.1016/S0264-3707(99)00041-1.
Tavarnelli, E., Holdsworth, R.E., Clegg, P., Jones, R., and McCaffrey, K.W., 2004, The anatomy and evolution of a transpressional imbricate zone, Southern Uplands, Scotland: Journal of Structural Geology, v. 26, p. 1341–1360, https://doi.org/10.1016/j.jsg.2004.01.003.
Teyssier, C., and Tikoff, B., 1998, Strike-slip partitioned transpression of the San Andreas fault system: A lithospheric scale approach, *in* Holdsworth, R.E., Strachan, R.A., and Dewey, J.F., eds., Continental Transpressional and Transtensional Tectonics: Geological Society, London, Special Publication 135, p. 143–158, https://doi.org/10.1144/GSL.SP.1998.135.01.10.
Tikoff, B., and Teyssier, C., 1994, Strain modeling of displacement field partitioning in transpressional orogens: Journal of Structural Geology, v. 16, no. 11, p. 1575–1588, https://doi.org/10.1016/0191-8141(94)90034-5.
Titus, S.J., Housen, B., and Tikoff, B., 2007, A kinematic model for the Rinconada fault system in central California based on structural analysis of en échelon folds and paleomagnetism: Journal of Structural Geology, v. 29, p. 961–982, https://doi.org/10.1016/j.jsg.2007.02.004.
Wakabayashi, J., Hengesh, J.V., and Sawyer, T.L., 2004, Four dimensional transform fault processes: Progressive evolution of stepovers and bends: Tectonophysics, v. 392, p. 279–301, https://doi.org/10.1016/j.tecto.2004.04.013.
Wilcox, R.E., Harding, T.P., and Seely, D.R., 1973, Basic wrench tectonics: American Association of Petroleum Geologists Bulletin, v. 57, p. 74–96.
Williams, P., Sykes, L., Nicholson, C., and Seeber, L., 1990, Seismotectonics of the easternmost Transverse Ranges California: Relevance for seismic potential of the San Andreas fault: Tectonics, v. 9, p. 185–204, https://doi.org/10.1029/TC009i001p00185.
Winker, C.D., and Kidwell, S.M., 1996, Stratigraphy of a marine rift basin: Neogene of the western Salton Trough, California, *in* Abbott, P.L., and Cooper, J.D., eds., Field Conference Guidebook and Volume for American Association of Petroleum Geologists Annual Convention: Bakersfield, California, Pacific Section, American Association of Petroleum Geologists, p. 295–336.
Woodcock, N.H., and Fischer, M., 1986, Strike-slip duplexes: Journal of Structural Geology, v. 8, p. 725–735, https://doi.org/10.1016/0191-8141(86)90021-0.
Yule, D., 2009, The enigmatic San Gorgonio Pass: Geology, v. 37, no. 2, p. 191–192, https://doi.org/10.1130/focus022009.1.
Zeeden, C., Rivera, T.A., and Storey, M., 2014, An astronomical age for the Bishop Tuff and concordance with radioisotopic dates: Geophysical Research Letters, v. 41, p. 3478–3484, https://doi.org/10.1002/2014GL059899.
Zoback, M.E., Zoback, M.L., Mount, V.S., Suppe, J., Eaton, J.P., Healy, J.H., Oppenheimer, D., Reasenberg, P., Jones, L., Raleigh, C.B., Wong, I., Scotti, O., and Wentworth, C., 1987, New evidence on the state of stress of the San Andreas fault system: Science, v. 238, p. 1105–1111, https://doi.org/10.1126/science.238.4830.1105.